Journal of Sound and Vibration 527 (2022) 116809

Contents lists available at ScienceDirect

Journal of Sound and Vibration

journal homepage: www.elsevier.com/locate/jsvi

Flexural–flexural internal resonances 3:1 in initially straight, extensible Timoshenko beams with an axial spring ☆

Lukasz Kloda [a,*], Stefano Lenci [b], Jerzy Warminski [a], Zofia Szmit [a]

[a] Department of Applied Mechanics, Lublin University of Technology, ul. Nadbystrzycka 36, 20-618 Lublin, Poland
[b] Department of Civil and Buildings Engineering, and Architecture, Polytechnic University of Marche, via Brecce Bianche, 60131 Ancona, Italy

ARTICLE INFO

Keywords:
Nonlinear vibrations
3:1 internal resonance
Multiple time scale method
Extensible-shearable planar beam
Transversal–longitudinal coupling
Energy transfer

ABSTRACT

This work investigates the dynamics of a hinged–simply supported beam with an axial spring in the neighbourhood of a 3:1 internal resonance between two successive transversal vibration modes. Multiple time scale method is applied to the analytical model of the planar extensible-shearable beam with associated boundary conditions, and a second order approximate solution is obtained. The phenomena that we investigate occur on the resonant branch of the frequency response curve around the main natural frequency, and consists of a localized extra (bent) peak on that branch. Also some detached branches have been theoretically detected in the neighbourhood of this extra peak. The analytical frequency response curves are analysed extensively and have been compared with finite element numerical simulations, finding an overall good agreement. Stability of the analytical solutions is checked by computing the eigenvalues of the Jacobian matrix and looking at the sign of their real part. Strain energies due to flexural, axial, shear deformability and axial spring are determined and compared between each other to ascertain their relative importance.

1. Introduction

In engineering the most common structural elements are cables, beams, plates or shells, which are applied in tall buildings, slender bridges, helicopter blades, aeroplane wings, cars and so on. During operation time, these structures are subjected to external dynamical loads, and their most dangerous behaviour is in the dynamical realm. In general, small amplitudes dynamic response is modelled using linear vibration theory. As the amplitude of system response increases, linear models are no longer valid, and material as well as geometric nonlinearities have to be taken into account.

Large free and forced-damped nonlinear oscillations of beams with different boundary conditions are of practical as well as scientific interest, and have been studied in the past. A conventional combination of fixed, hinged, simply supported and free boundary conditions at the ends were presented in [1]. Generally (but not always), the clamped–simply supported and hinged–simply supported beams have softening nature (the vibration frequency decreases by increasing the amplitude of the motion); cantilever beam presents almost linear dynamic response, while axially restrained ends determine a strong hardening behaviour in the structure (the vibration frequency increases by increasing the amplitude of the motion). Softening on the frequency amplitude characteristic for structures with free axial displacement is the effect of axial inertia and geometric nonlinear balance terms [2–5].

To investigate the transition from axially unrestrained to restrained boundary conditions, Lenci et al. proposed an extensible-shearable beam model with axial spring fixed at the end. With the use of perturbation methods they studied the moderately large

☆ This document is the results of the research project no. 2019/33/N/ST8/02661 funded by the National Science Centre, Poland.
* Corresponding author.
E-mail address: l.kloda@pollub.pl (L. Kloda).

https://doi.org/10.1016/j.jsv.2022.116809
Received 2 September 2021; Received in revised form 27 January 2022; Accepted 28 January 2022
Available online 18 February 2022

free nonlinear oscillations [6,7] and forced-damped vibrations for the first [8] and higher order resonances [9]. Hardening/softening dichotomy for the parametrically excited beam–spring system were experimentally tested in [10,11], while qualitative and quantitative agreement between theoretical/numerical and experimental results were obtained for kinematically excited beams in [12,13].

Analogous to systems with more than one degree of freedom, nonlinear interactions between normal modes in continuous systems cause additional dynamic effects. Knowledge of internal resonances is well established in dynamical systems with quadratic and cubic nonlinearities [14–16]. Nonlinear response of parametrically excited, Euler–Bernoulli beam taking into account axial static load applied through the spring and hinged–clamped ends were studied in [17], and next the same configuration of the beam was improved by axial deformations in [18]. In their model, authors neglected shearing effects and longitudinal inertia and then, by varying pulling force, tuned the first and second natural frequencies to the desired multiplier. In a similar arrangement, natural frequencies and nonlinear mode interactions for buckled clamped–clamped beam were investigated in [19–21].

Apart from buckled beams, modal interactions are observed in initially curved (shallow) microelectromechanical systems, which can be additionally actuated by static and dynamic electric forces [22]. Another opportunity to match the natural frequencies in an integer ratio are thermomechanical couplings in thermal environments as a parameter is varied [23]. Flexural–flexural interactions occur also in cantilever beams under gravitational effect [24], as well as in initially straight and predeformed rotating structures subjected to centrifugal forces [25–27]. Alfosail and Younis shed the light on internal resonances in inclined riser, which undergoes environmental forces, more precisely vortex induced vibrations [28]. In axially moving beams, by properly tuning the constant beam velocity the condition of internal resonance was achieved [29]. In the initially straight beam model, one important phenomenon is the transversal–longitudinal internal resonance, in which natural frequencies are very close to ratio $2:1$ ($2\omega_{0,n} \approx \omega_A$) [30]. External action applied to the structure only in the transversal direction stimulates large flexural amplitudes, and indirectly longitudinal oscillations through geometric nonlinearities and inertia terms. For precisely selected parameters of the structure, energy transfer between the two orthogonal directions occurred [31,32].

In this paper we focused on modal interactions in the hinged–simply supported beams with an axial spring at one end. The stiffness of the spring is the passive control parameter, which is chosen to have $3:1$ ratio ($3\tilde{\omega}_{0,n} \approx \tilde{\omega}_{0,m}$) between two different *flexural* modes. In fact, for this structural system only 2:1 flexural–longitudinal internal resonance was investigated [30], while *transversal–transversal* resonance is studied here for the first time (to the best of authors knowledge), extending the study on nonlinear response of the *separated* (i.e. without internal resonance) first seven flexural modes presented in [8].

It is worth to remark that if the frequency Ω of the periodic external excitation is close to a given natural frequency ω_n (so that we have external resonance from the load), and if $\omega_m \approx 3\omega_n$ by internal resonance, then $3\Omega \approx \omega_m$ and so the mode m is subjected to superharmonic resonance (see Sect. 4.1.3 of [15]). Thus, it is not immediately clear if the activation (i.e. *large* displacements) of the m mode is due to coupling between modes (internal resonance) or *directly* to the superharmonic resonance. To show that the former case happens, we consider also an external excitation that does *not* solicit the mode m (practically we consider a concentrated force in a node of the mth linear mode shape), so that its activation is possible, at least in this case, because of the coupling between modes due to the internal resonance.

As we will see in due course, in the considered modal coupling between two different flexural modes, a certain role plays the axial motion, that naturally appears at the second order and that contributes to the exchange of energy/motion between flexural modes, acting as a kind of "carrier" (roughly speaking).

The main motivation of this paper is to detect analytically a phenomenon of the born of a secondary peak on the primary nonlinear resonance branches, that has been numerically observed in several previous works [8,9,31,33].

The manuscript is organized as follows. In Section 2 the mathematical description of the hinged–simply supported beam with an axial spring is presented. Section 3 contains the multiple time scale method (MTSM) application up to cubic nonlinearities and second order approximation. Analytical outcomes and stability analysis of dynamical response are compared with numerical simulations in Section 4 to check the reliability of the approximate analytical solution. Section 5 stresses the contribution of the work.

2. Problem formulation

Let us consider a planar extensible Timoshenko beam, which is made of homogeneous material defined by Young's modulus E, shear modulus G and density ρ. Dimensions of the initially straight structure are: length L, cross-sectional area A and second moment of area J. Space and time dependent terms $W(Z,T)$ and $U(Z,T)$ describe displacements in longitudinal and transversal directions, respectively. Furthermore, rotation angle of the cross section $\theta(Z,T)$ takes into account sum of slope angle of the axis of the beam and shear deformation, but warping effect of the cross-section is neglected in the analysis. The beam is subjected to longitudinal, transversal and rotational inertia. It is assumed that a linear viscous damping acts on the beam and, accordingly, the three dissipation factors C_W, C_U and C_θ are considered. Moreover, periodic external excitation $P_U(Z)\cos(\Omega T)$ is introduced in the transverse direction, to directly stimulate only flexural modes. The beam model is governed by the three nonlinear partial differential equations:

$$\rho A\ddot{W} + C_W\dot{W} = \left\{ EA\left[\sqrt{(1+W')^2+U'^2}-1\right]\frac{1+W'}{\sqrt{(1+W')^2+U'^2}} + GA\left[\theta - \arctan\left(\frac{U'}{1+W'}\right)\right]\frac{U'}{\sqrt{(1+W')^2+U'^2}} \right\}', \tag{1}$$

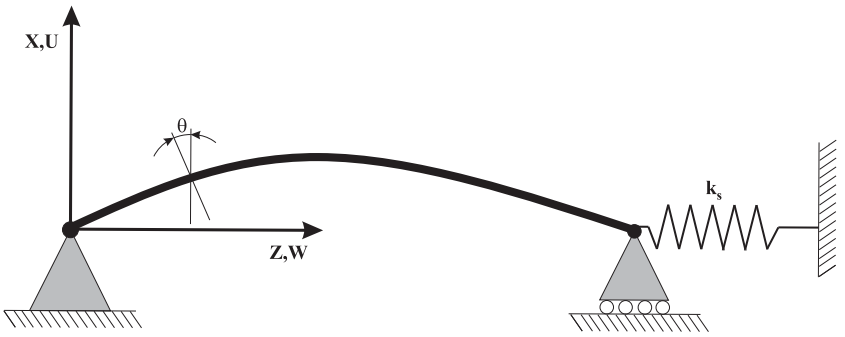

Fig. 1. The beam–spring system.

$$\rho A\ddot{U} + C_U\dot{U} + P_U(Z)\cos(\Omega T) = \left\{ EA\left[\sqrt{(1+W')^2+U'^2}-1\right]\frac{U'}{\sqrt{(1+W')^2+U'^2}} - GA\left[\theta - \arctan\left(\frac{U'}{1+W'}\right)\right]\frac{1+W'}{\sqrt{(1+W')^2+U'^2}}\right\}', \tag{2}$$

$$\rho J\ddot{\theta} + C_\theta\dot{\theta} = \left[EJ\frac{\theta'}{\sqrt{(1+W')^2+U'^2}}\right]' - GA\left[\theta - \arctan\left(\frac{U'}{1+W'}\right)\right]\sqrt{(1+W')^2+U'^2}, \tag{3}$$

where Newton's and Lagrange's notation are used $\left(\frac{d(...)}{dt} = (\dot{...}), \quad \frac{d(...)}{dZ} = (...)'\right)$. We refer to [6,8] for more details on the derivation of the previous equations.

Six boundary conditions correspond to the scheme presented in Fig. 1 and involves free rotation, restrained displacements of the beams ends and the axial elastic support:

at $Z = 0$

$$W = 0, \quad U = 0, \quad M = 0, \tag{4}$$

at $Z = L$

$$EA\left[\sqrt{(1+W')^2+U'^2}-1\right]\frac{1+W'}{\sqrt{(1+W')^2+U'^2}} + GA\frac{\left[\theta - \arctan\left(\frac{U'}{1+W'}\right)\right]U'}{\sqrt{(1+W')^2+U'^2}} + k_s W = 0, \quad U = 0, \quad M = 0, \tag{5}$$

where M is the bending moment, proportional to geometric curvature $M = EJ\frac{\theta'}{\sqrt{(1+W')^2+U'^2}}$ [34], and k_s is the stiffness of the spring (see Fig. 1). Note that $M = 0$ implies $\theta' = 0$. For simplicity time and space dependent notation is omitted in Eqs. (1)–(5).

3. Multiple time scales method

The system described in Section 2 is solved analytically with the help of the multiple time scale method in the neighbourhood of a primary flexural mode n (which is directly excited by the external force), considering 3 to 1 modal interaction with a secondary flexural mode m.

In this work we seek the approximate solution only up to cubic geometric nonlinearities, so that we can expand up to the third order the governing equations. Higher order terms can be included in future work, even if we emphasize that this restriction is mainly caused by limitations of the commercial manipulator Mathematica© we used for the computations. Thus, Eqs. (1)–(5) take the form:

$$\rho A\ddot{W} + C_W\dot{W} = EA\left(W' + \frac{1}{2}U'^2 - U'^2\,W'\right)' + GA\left(U'\theta - U'^2 + 2U'^2W' - U'W'\theta\right)', \tag{6}$$

$$\rho A\ddot{U} + C_U\dot{U} + P_U(Z)\cos(\Omega T) = EA\left(U'W' + \frac{1}{2}U'^3 - U'W'^2\right)' + GA\left(U' - \theta - U'W' + \frac{1}{2}U'^2\theta - \frac{5}{6}U'^3 + U'W'^2\right)', \tag{7}$$

$$\rho J\ddot{\theta} + C_\theta\dot{\theta} = EJ\left(\theta' - W'\theta' - \frac{1}{2}U'^2\theta'\right)' + GA\left(U' - \theta - W'\theta - \frac{1}{2}U'^2\theta + \frac{1}{6}U'^3\right), \tag{8}$$

with boundary conditions at $Z = 0$

$$W = 0, \quad U = 0, \quad \theta' = 0, \tag{9}$$

and boundary conditions at $Z = L$

$$EA\left(W' + \frac{1}{2}U'^2 - U'^2\ W'\right) + GA\left(U'\theta - U'^2 + 2U'^2W' - U'W'\theta\right) + k_sW = 0, \quad U = 0, \quad \theta' = 0. \tag{10}$$

A formal small book-keeping parameter is introduced to consistently separate three time scales: fast t_0, slower t_1 and the slowest t_2:

$$t_0 = T,\ t_1 = \varepsilon T,\ t_2 = \varepsilon^2 T. \tag{11}$$

As generally established in the multiple time scale method, variables and their time derivatives are sought after in the form:

$$\begin{aligned}
&W(Z,T) = \varepsilon W_1(Z,t_0,t_1,t_2) + \varepsilon^2 W_2(Z,t_0,t_1,t_2) + \varepsilon^3 W_3(Z,t_0,t_1,t_2),\\
&U(Z,T) = \varepsilon U_1(Z,t_0,t_1,t_2) + \varepsilon^2 U_2(Z,t_0,t_1,t_2) + \varepsilon^3 U_3(Z,t_0,t_1,t_2),\\
&\theta(Z,T) = \varepsilon \theta_1(Z,t_0,t_1,t_2) + \varepsilon^2 \theta_2(Z,t_0,t_1,t_2) + \varepsilon^3 \theta_3(Z,t_0,t_1,t_2),
\end{aligned} \tag{12}$$

$$\begin{aligned}
&\dot{W}(Z,T) = D_0W(Z,T) + \varepsilon D_1W(Z,T) + \varepsilon^2 D_2W(Z,T),\\
&\ddot{W}(Z,T) = D_0^2W(Z,T) + \varepsilon 2D_0D_1W(Z,T) + \varepsilon^2\left(2D_0D_2 + D_1^2\right)W(Z,T),\\
&\dot{U}(Z,T) = D_0U(Z,T) + \varepsilon D_1U(Z,T) + \varepsilon^2 D_2U(Z,T),\\
&\ddot{U}(Z,T) = D_0^2U(Z,T) + \varepsilon 2D_0D_1U(Z,T) + \varepsilon^2\left(2D_0D_2 + D_1^2\right)U(Z,T),\\
&\dot{\theta}(Z,T) = D_0\theta(Z,T) + \varepsilon D_1\theta(Z,T) + \varepsilon^2 D_2\theta(Z,T),\\
&\ddot{\theta}(Z,T) = D_0^2\theta(Z,T) + \varepsilon 2D_0D_1\theta(Z,T) + \varepsilon^2\left(2D_0D_2 + D_1^2\right)\theta(Z,T),
\end{aligned} \tag{13}$$

where $D_0 - D_2$ represent Nayfeh notation and correspond to time derivatives with respect to previously introduced time scales $t_0 - t_2$ [15,35,36]. As customary, damping coefficients and excitation amplitude are rescaled as follows

$$C_W = \varepsilon^2 c_W,\ C_U = \varepsilon^2 c_U,\ C_\theta = \varepsilon^2 c_\theta,\ P_U(Z) = \varepsilon^3 p_U(Z). \tag{14}$$

Substituting Eqs. (11)–(14) into Eqs. (6)–(10) we get a set of equations, which will be solved sequentially:

First order

$$EAW_1'' - \rho AD_0^2W_1 = 0, \quad GA(U_1' - \theta_1)' - \rho AD_0^2U_1 = 0, \quad EJ\theta_1'' - GA(\theta_1 - U_1') - \rho J D_0^2\theta_1 = 0. \tag{15}$$

Boundary conditions:

$$\begin{aligned}
&W_1(0) = 0, \quad U_1(0) = 0, \quad \theta_1'(0) = 0,\\
&k_sW_1(L) + EAW_1'(L) = 0, \quad U_1(L) = 0, \qquad \theta_1'(L) = 0.
\end{aligned} \tag{16}$$

Second order

$$EAW_2'' - \rho AD_0^2W_2 = 2\rho AD_0D_1W_1 - GA(\theta_1U_1' - U_1'^2)' - \frac{1}{2}EA(U_1'^2)', \tag{17}$$

$$GA(U_2' - \theta_2)' - \rho AD_0^2U_2 = 2\rho AD_0D_1U_1 - EA(U_1'W_1')' + GA(U_1'W_1')', \tag{18}$$

$$EJ\theta_2'' - GA(\theta_2 - U_2') - \rho J D_0^2\theta_2 = 2\rho J D_0D_1\theta_1 + GA(W_1'\theta_1) + EJ(W_1'\theta_1')'. \tag{19}$$

Boundary conditions:

$$\begin{aligned}
&W_2(0) = 0, \quad U_2(0) = 0, \quad \theta_2'(0) = 0,\\
&k_sW_2(L) + EAW_2'(L) + \frac{1}{2}EAU_1'^2(L) - GA[U_1'^2(L) + \theta_1(L)U_1'(L)] = 0, \quad U_2(L) = 0, \quad \theta_2'(L) = 0.
\end{aligned} \tag{20}$$

Third order

$$\begin{aligned}
&EAW_3'' - \rho AD_0^2W_3 = c_W D_0W_1 + \rho A(D_1^2 + 2D_0D_2)W_1 + 2\rho AD_0D_1W_2 - EA(U_1'U_2' - U_1'^2W_1')'\\
&- GA(2W_1'U_1'^2 + \theta_2U_1' - 2U_2'U_1' - \theta_1W_1'U_1' + \theta_1U_2')',
\end{aligned} \tag{21}$$

$$\begin{aligned}
&GA(U_3' - \theta_3)' - \rho AD_0^2U_3 = c_U D_0U_1 + p_U(Z)\cos(\Omega T) + \rho A(2D_0D_2 + D_1^2)U_1 + 2\rho AD_0D_1U_2\\
&+ EA\left(U_1'W_1'^2 - U_1'W_2' - \frac{1}{2}U_1'^3 - U_2'W_1'\right)' + GA\left(-\frac{1}{2}\theta_1U_1'^2 - U_1W_1'^2 + U_1'W_2' + \frac{5}{6}U_1'^3 + U_2'W_1'\right)',
\end{aligned} \tag{22}$$

$$\begin{aligned}
&EJ\theta_3'' - GA\left(\theta_3 - U_3'\right) - \rho J D_0^2\theta_3 = c_\theta D_0\theta_1 + \rho J\left(2D_0D_2 + D_1^2\right)\theta_1 + \rho J2D_0D_1\theta_2\\
&+ GA\left(\frac{1}{2}\theta_1U_1'^2 - \frac{1}{6}U_1'^3 + \theta_2W_1' + \theta_1W_2'\right) + EJ\left(\frac{1}{2}\theta_1'U_1'^2 - \theta_1'W_1'^2 + \theta_2'W_1' + \theta_1'W_2'\right)'.
\end{aligned} \tag{23}$$

Boundary conditions:

$$W_3(0) = 0, \quad U_3(0) = 0, \quad \theta_3'(0) = 0,$$

$$k_s W_3(L) + EAW_3'(L) + GA\left[-\theta_1(L)W_1'(L)U_1'(L) + \theta_2(L)U_1'(L) + U_2'(L)\theta_1(L)\right] + (EA - 2GA)[U_2'(L)U_1'(L) - W_1'(L)U_1'^2(L)] = 0,$$
$$U_3(L) = 0, \quad \theta_3'(L) = 0. \tag{24}$$

In the perspective of two modes interaction, we assume a multiplicative ratio equal to 3 between two natural frequencies ω_m and ω_n. A small detuning, measured by the parameter σ_1, is introduced to take into account the closeness of ω_m and $3\omega_n$, i.e. the non perfect internal resonance. Furthermore, we impose that the frequency of excitation is in the vicinity of the primary resonance ω_n, detuned by a second additive parameter σ_2 [17]:

$$\omega_m T = (3\omega_n + \epsilon^2\sigma_1)T = 3\omega_n t_0 + \sigma_1 t_2, \quad \Omega T = (\omega_n + \epsilon^2\sigma_2)T = \omega_n t_0 + \sigma_2 t_2. \tag{25}$$

Note that $\omega_m T = 3\Omega_n T - (3\sigma_2 - \sigma_1)t_2$, so that $(3\sigma_2 - \sigma_1)$ is the detuning for the superharmonic resonance of the mode m.

The above assumptions will be applied directly to the third order solution in Section 3.3.

3.1. First order solutions

Excluding the case of internal longitudinal–transversal resonance discussed in [30], in the present investigation on transversal–transversal internal resonance we assume longitudinal deformation to be negligible to the first-order equation. This is confirmed by forthcoming FE simulations, where it is shown that axial displacements are (at least) one order of magnitude smaller than the transversal one (see Fig. 5). Similar procedure was used in [6,8,9,31], but not in [7,30]:

$$W_1(Z,T) = 0. \tag{26}$$

This assumption simplifies the higher order problems, but does not eliminate geometrical coupling between axial and transversal directions of Eqs. (17)–(23). The general solution of the linear problem (15)–(16) for the nth and mth flexural modes are time and space dependent, and consists of two flexural mode shapes $\hat{U}_{1,n}(Z)$, $\hat{U}_{1,m}(Z)$ and $\hat{\theta}_{1,n}(Z)$, $\hat{\theta}_{1,m}(Z)$, multiplied by complex amplitudes and corresponding (fast) time harmonic functions $e^{i\omega_n t_0}$, $e^{i\omega_m t_0}$

$$U_1(Z,t_0,t_1,t_2) = A_1(t_1,t_2)e^{i\omega_n t_0}\hat{U}_{1,n}(Z) + A_2(t_1,t_2)e^{i\omega_m t_0}\hat{U}_{1,m}(Z) + c.c, \tag{27}$$

$$\theta_1(Z,t_0,t_1,t_2) = A_1(t_1,t_2)e^{i\omega_n t_0}\hat{\theta}_{1,n}(Z) + A_2(t_1,t_2)e^{i\omega_m t_0}\hat{\theta}_{1,m}(Z) + c.c, \tag{28}$$

where i is the imaginary unit and c.c. represents complex conjugate. The nth mode shape and associated natural frequency are given by

$$\hat{U}_{1,n}(Z) = \sin\left(\frac{n\pi Z}{L}\right), \quad \hat{\theta}_{1,n}(Z) = \left(\frac{n\pi}{L} - \frac{L\rho\omega_n^2}{\pi G n}\right)\cos\left(\frac{n\pi Z}{L}\right),$$
$$\omega_n = \sqrt{AGL^2 + \pi^2 n^2(E+G)J - \sqrt{\left[AGL^2 + \pi^2 J n^2(E+G)\right]^2 - 4\pi^4 EGJ^2 n^4}}, \tag{29}$$

and mth mode can be read by substitution $n \to m$. For a detailed derivation of mode shapes and natural frequencies we refer to [6,7].

3.2. Second order solution

The solution of the second order problem in the axial direction (17) with associated boundary conditions (20) can be decomposed into space functions, (slow) time dependent amplitudes and harmonic (fast) time functions, and is given by (the overbar stands for complex conjugate):

$$W_2(Z,t_0,t_1,t_2) = W_{2a}(Z)A_1(t_1,t_2)\bar{A}_1(t_1,t_2) + W_{2b}(Z)A_2(t_1,t_2)\bar{A}_2(t_1,t_2) + W_{2c}(Z)A_1^2(t_1,t_2)e^{2i\omega_n t_0} + W_{2d}(Z)A_2^2(t_1,t_2)e^{2i\omega_m t_0}$$
$$+ W_{2e}(Z)A_1(t_1,t_2)A_2(t_1,t_2)e^{i(\omega_n+\omega_m)t_0} + W_{2f}(Z)A_1(t_1,t_2)\bar{A}_2(t_1,t_2)e^{i(\omega_n-\omega_m)t_0} + c.c. \tag{30}$$

The functions $W_{2a}(Z)$, $W_{2b}(Z)$, $W_{2c}(Z)$, $W_{2d}(Z)$, $W_{2e}(Z)$ and $W_{2f}(Z)$ are real valued and reported in Appendix A. They quantify how the first order transversal motion U_1 and θ_1 induce a second order axial motion W_2, through which the modal coupling is successively activated (at the third order). Note that since we are not considering 2:1 internal resonance (which is instead addressed in [30]), we have no secular terms in the expression (30).

To look for the solution of the second order problem in the transversal direction we rewrite Eqs. (18)–(19) taking into account Eqs. (26)–(28):

$$GA(U_2' - \theta_2)' - \rho A D_0^2 U_2 = 2\rho A\left[i\omega_n\frac{\partial A_1(t_1,t_2)}{\partial t_1}e^{i\omega_n t_0}\hat{U}_{1,n}(Z) + i\omega_m\frac{\partial A_2(t_1,t_2)}{\partial t_1}e^{i\omega_m t_0}\hat{U}_{1,m}(Z)\right] + c.c., \tag{31}$$

$$EJ\theta_2'' - GA(\theta_2 - U_2') - \rho J D_0^2\theta_2 = 2\rho J\left[i\omega_n\frac{\partial A_1(t_1,t_2)}{\partial t_1}e^{i\omega_n t_0}\hat{\theta}_{1,n}(Z) + i\omega_m\frac{\partial A_2(t_1,t_2)}{\partial t_1}e^{i\omega_m t_0}\hat{\theta}_{1,m}(Z)\right] + c.c. \tag{32}$$

The right hand sides of the previous equations suggest to assume

$$U_2(Z,t_0,t_1,t_2) = e^{i\omega_n t_0}U_{2,n}(Z,t_1,t_2) + e^{i\omega_m t_0}U_{2,m}(Z,t_1,t_2) + c.c., \tag{33}$$

$$\theta_2(Z,t_0,t_1,t_2) = e^{i\omega_n t_0}\theta_{2,n}(Z,t_1,t_2) + e^{i\omega_m t_0}\theta_{2,m}(Z,t_1,t_2) + c.c. \tag{34}$$

Inserting Eqs. (33)–(34) in Eqs. (31)–(32), and considering only the terms multiplying $e^{i\omega_n t_0}$, we obtain

$$GA(U'_{2,n} - \theta_{2,n})' + \rho A\omega_n^2 U_{2,n} = 2\rho A i\omega_n \frac{\partial A_1(t_1,t_2)}{\partial t_1}\hat{U}_{1,n}(Z), \tag{35}$$

$$EJ\theta''_{2,n} - GA(\theta_{2,n} - U'_{2,n}) + \rho J\omega_n^2\theta_{2,n} = 2\rho J i\omega_n \frac{\partial A_1(t_1,t_2)}{\partial t_1}\hat{\theta}_{1,n}(Z). \tag{36}$$

The solvability condition of the previous equations is obtained by multiplying by $\hat{U}_{1,n}$ and $\hat{\theta}_{1,n}$, and integrating over the spatial domain:

$$\int_0^L \left[GA\left(U'_{2,n} - \theta'_{2,n}\right)' + \rho A\omega_n^2 U_{2,n}\right]\hat{U}_{1,n}dZ = 2\rho A i\omega_n \frac{\partial A_1(t_1,t_2)}{\partial t_1}\int_0^L \left(\hat{U}_{1,n}\right)^2 dZ, \tag{37}$$

$$\int_0^L \left[EJ\theta''_{2,n} - GA\left(\theta_{2,n} - U'_{2,n}\right) + \rho J\omega_n^2\theta_{2,n}\right]\hat{\theta}_{1,n}dZ = 2\rho J i\omega_n \frac{\partial A_1(t_1,t_2)}{\partial t_1}\int_0^L \left(\hat{\theta}_{1,n}\right)^2 dZ. \tag{38}$$

Integrating by parts Eqs. (37)–(38), using boundary conditions Eq. (20), and summing up the two equations we obtain

$$\int_0^L \left[GA\left(\hat{U}'_{1,n} - \hat{\theta}'_{1,n}\right)' + \rho A\omega_n^2\hat{U}_{1,n}\right]U_{2,n}dZ + \int_0^L \left[EJ\hat{\theta}''_{1,n} - GA\left(\hat{\theta}_{1,n} - \hat{U}'_{1,n}\right) + \rho J\omega_n^2\hat{\theta}_{1,n}\right]\theta_{2,n}dZ =$$
$$2\rho i\omega_n \frac{\partial A_1(t_1,t_2)}{\partial t_1}\left[A\int_0^L \left(\hat{U}_{1,n}\right)^2 dZ + J\int_0^L \left(\hat{\theta}_{1,n}\right)^2 dZ\right]. \tag{39}$$

It is easy to see that functions in brackets on the left hand side are solutions of the first order problem and thus vanish. Since the integrals on the right hand side are positive, it follows that

$$\frac{\partial A_1(t_1,t_2)}{\partial t_1} = 0. \tag{40}$$

Suchlike derivation is repeated for the other harmonic $e^{i\omega_m}$ leading to

$$\frac{\partial A_2(t_1,t_2)}{\partial t_1} = 0. \tag{41}$$

Then, complex amplitudes do not depend on the slow time t_1, although they depend on second slowest time-scale, $A_1(t_2)$ and $A_2(t_2)$. Now Eqs. (18)–(19) are reduced to

$$GA(\theta_2 - U'_2)' + \rho A D_0^2 U_2 = 0, \quad EJ\theta''_2 - GA(\theta_2 - U'_2) - \rho J D_0^2\theta_2 = 0. \tag{42}$$

The solutions of these homogeneous equations are already presented in the first order solution (27)–(28), thus we can assume the second order solution as

$$U_2(Z,t_0,t_1,t_2) = 0, \quad \theta_2(Z,t_0,t_1,t_2) = 0. \tag{43}$$

3.3. Third order solution

For the purpose of this work it is not needed to determine the third order solution. It is sufficient to use the solvability conditions of the equation governing the transversal motion. Using the results of the previous sections, the third order Eqs. (22)–(23) become

$$\begin{aligned}
&GA(U'_3 - \theta_3)' - \rho A D_0^2 U_3 = ic_U\left[\omega_n\hat{U}_{1,n}(Z)A_1(t_2)e^{i\omega_n t_0} + \omega_m\hat{U}_{1,m}(Z)A_2(t_2)e^{i\omega_m t_0}\right]\\
&+ 2i\rho A\left[\hat{U}_{1,n}(Z)\omega_n\frac{\partial A_1(t_2)}{\partial t_2}e^{i\omega_n t_0} + \hat{U}_{1,m}(Z)\omega_m\frac{\partial A_2(t_2)}{\partial t_2}e^{i\omega_m t_0}\right] + U_{3a}(Z)A_1^2(t_2)\bar{A}_1(t_2)e^{i\omega_n t_0}\\
&+ U_{3b}(Z)A_1(t_2)A_2(t_2)\bar{A}_2(t_2)e^{i\omega_n t_0} + U_{3c}(Z)A_1^2(t_2)\bar{A}_2(t_2)e^{i(2\omega_n t_0 - \omega_m t_0)} + U_{3d}(Z)A_1(t_2)\bar{A}_1(t_2)A_2(t_2)e^{i\omega_m t_0}\\
&+ U_{3e}(Z)A_2^2(t_2)\bar{A}_2(t_2)e^{i\omega_m t_0} + U_{3f}(Z)A_1^3(t_2)e^{3i\omega_n t_0} + \frac{1}{2}p_U(Z)e^{i(\omega_n t_0 + \sigma_2 t_2)} + \mathrm{NST} + c.c,
\end{aligned} \tag{44}$$

$$\begin{aligned}
&EJ\theta''_3 - GA\left(\theta_3 - U'_3\right) - \rho J D_0^2\theta_3 = ic_\theta\left[\omega_n\hat{\theta}_{1,n}(Z)A_1(t_2)e^{i\omega_n t_0} + \omega_m\hat{\theta}_{1,m}(Z)A_2(t_2)e^{i\omega_m t_0}\right]\\
&+ 2i\rho J\left[\hat{\theta}_{1,n}(Z)\omega_n\frac{\partial A_1(t_2)}{\partial t_2}e^{i\omega_n t_0} + \hat{\theta}_{1,m}(Z)\omega_m\frac{\partial A_2(t_2)}{\partial t_2}e^{i\omega_m t_0}\right] + \theta_{3a}(Z)A_1^2(t_2)\bar{A}_1(t_2)e^{i\omega_n t_0}\\
&+ \theta_{3b}(Z)A_1(t_2)A_2(t_2)\bar{A}_2(t_2)e^{i\omega_n t_0} + \theta_{3c}(Z)A_1^2(t_2)\bar{A}_2(t_2)e^{i(2\omega_n t_0 - \omega_m t_0)} + \theta_{3d}(Z)A_1(t_2)\bar{A}_1(t_2)A_2(t_2)e^{i\omega_m t_0}\\
&+ \theta_{3e}(Z)A_2^2(t_2)\bar{A}_2(t_2)e^{i\omega_m t_0} + \theta_{3f}(Z)A_1^3(t_2)e^{3i\omega_n t_0} + \mathrm{NST} + c.c.
\end{aligned} \tag{45}$$

where

$$\cos(\Omega T) = \frac{e^{i\Omega T} + e^{-i\Omega T}}{2} = \frac{e^{i(\omega_n t_0 + \sigma_2 t_2)} + e^{-i(\omega_n t_0 + \sigma_2 t_2)}}{2} = \frac{e^{i(\omega_n t_0 + \sigma_2 t_2)}}{2} + c.c. \tag{46}$$

is used. Space dependent functions $U_{3a}(Z) - U_{3f}(Z)$ and $\theta_{3a}(Z) - \theta_{3f}(Z)$ are reported in Appendix B. They depend on W_2, and this shows how the second order axial solution affects the third order transverse motion. However, there are also terms depending on

Table 1
Mechanical properties of the beam.

A, m^2	L, m	E, GPa	υ, (–)	χ, (–)	ρ, kg/m^3
0.05×0.05	0.5	210	0.3	0.85	7580

U_1 only, and thus we cannot conclude that the coupling between flexural modes is only due to the axial motion, even if this seems to play the major role. The coupling terms are those multiplying $A_1(t_2)$ and $A_2(t_2)$, namely U_{3b}, U_{3c}, U_{3d}, θ_{3b}, θ_{3c} and θ_{3d}.

Using the resonance Eqs. (25) and collecting the exponential terms, Eqs. (44)–(45) become

$$\begin{aligned} GA(U_3' - \theta_3)' - \rho A D_0^2 U_3 = e^{i\omega_n t_0} \Big[& ic_U \omega_n \hat{U}_{1,n}(Z) A_1(t_2) + 2i\rho A \hat{U}_{1,n}(Z) \omega_n \frac{\partial A_1(t_2)}{\partial t_2} + U_{3a}(Z) A_1^2(t_2) \bar{A}_1(t_2) \\ & + U_{3b}(Z) A_1(t_2) A_2(t_2) \bar{A}_2(t_2) + U_{3c}(Z) \bar{A}_1^2(t_2) A_2(t_2) e^{i\sigma_1 t_2} + \frac{1}{2} p_U(Z) e^{i\sigma_2 t_2} \Big] \\ + e^{i\omega_m t_0} \Big[& ic_U \omega_m \hat{U}_{1,m}(Z) A_2(t_2) + 2i\rho A \hat{U}_{1,m}(Z) \omega_m \frac{\partial A_2(t_2)}{\partial t_2} + U_{3d}(Z) A_1(t_2) \bar{A}_1(t_2) A_2(t_2) \\ & + U_{3e}(Z) A_2^2(t_2) \bar{A}_2(t_2) + U_{3f}(Z) A_1^3(t_2) e^{-i\sigma_1 t_2} \Big] + \mathrm{NST} + c.c, \end{aligned} \tag{47}$$

$$\begin{aligned} EJ\theta_3'' - GA\left(\theta_3 - U_3'\right) - \rho J D_0^2 \theta_3 = e^{i\omega_n t_0} \Big[& ic_\theta \omega_n \hat{\theta}_{1,n}(Z) A_1(t_2) + 2i\rho J \hat{\theta}_{1,n}(Z) \omega_n \frac{\partial A_1(t_2)}{\partial t_2} + \theta_{3a}(Z) A_1^2(t_2) \bar{A}_1(t_2) \\ & + \theta_{3b}(Z) A_1(t_2) A_2(t_2) \bar{A}_2(t_2) + \theta_{3c}(Z) \bar{A}_1^2(t_2) A_2(t_2) e^{i\sigma_1 t_2} \Big] \\ + e^{i\omega_m t_0} \Big[& ic_\theta \omega_m \hat{\theta}_{1,m}(Z) A_2(t_2) + 2i\rho J \hat{\theta}_{1,m}(Z) \omega_m \frac{\partial A_2(t_2)}{\partial t_2} + \theta_{3d}(Z) A_1(t_2) \bar{A}_1(t_2) A_2(t_2) \\ & + \theta_{3e}(Z) A_2^2(t_2) \bar{A}_2(t_2) + \theta_{3f}(Z) A_1^3(t_2) e^{-i\sigma_1 t_2} \Big] + \mathrm{NST} + c.c, \end{aligned} \tag{48}$$

It is worth to remind that the external force $p_U(Z)$ appears only on the term multiplying $e^{i\omega_n t_0}$ of the first equation, because it is assumed to be in resonance with ω_n, see Eq. (25), and no distributed loads are considered. Thus, in the analytical computations only the nth mode is directly excited, while the mth mode is activated only by coupling due to the internal resonance. In forthcoming Finite Element (FE) numerical simulations, on the other hand, both modes are generally excited, and so it is not clear if the mth is activated by the internal resonance or by the superharmonic resonance. To check that the former case happens we will consider also a load $p_U(Z)$ not directly activating the mth mode, i.e. a concentrated force applied at a node of the mth mode shape.

By using the same procedure illustrated in Section 3.2 we obtain the solvability conditions of the Eqs. (47)–(48), which, after long computations, can be arranged as follows:

$$\frac{\partial A_1(t_2)}{\partial t_2} = c_1 c_U A_1(t_2) + c_2 c_\theta A_1(t_2) + 4ic_3 \bar{A}_1(t_2) A_1^2(t_2) + 4ic_4 e^{i\sigma_1 t_0} \bar{A}_1^2(t_2) A_2(t_2) + 4ic_5 A_1(t_2) \bar{A}_2(t_2) A_2(t_2) + \frac{1}{2} ic_6 F e^{i\sigma_2 t_2}, \tag{49}$$

$$\frac{\partial A_2(t_2)}{\partial t_2} = c_7 c_U A_2(t_2) + c_8 c_\theta A_2(t_2) + 4ic_9 A_1(t_2) \bar{A}_1(t_2) A_2(t_2) + 4ic_{10} \bar{A}_2(t_2) A_2^2(t_2) + 4ic_{11} e^{-i\sigma_1 t_2} A_1^3(t_2), \tag{50}$$

where

$$F = \int_0^L p_U(Z) \hat{U}_{1,n}(Z) dZ. \tag{51}$$

In the following we will considered only a concentrated force, of magnitude Q, at a given position $\bar{Z}$, i.e. $p_U(Z) = \delta(Z - \hat{Z})$ ($\delta(.)$ is the Dirac delta function), so that

$$F = Q \hat{U}_{1,n}(\bar{Z}). \tag{52}$$

In particular we will use $\bar{Z} = L/4$, which excites both first and second flexural modes, and $\bar{Z} = L/2$, which excites the first but not the second flexural mode.

The coefficients c_i depend on lower order solutions. c_1, c_2, c_7 and c_8 are related to damping, while c_6 to the excitation. All of them do not depend on the spring stiffness k_s. c_3 and c_{10} are, respectively, the nonlinear corrections coefficients of the nth and mth mode *alone*, i.e. in the absence of internal resonance. If negative, the corresponding mode is softening, otherwise it is hardening. c_4, c_5, c_9 and c_{11} are due to the coupling, and thus are very important for the present work; in fact, they are able to alter the hardening/softening behaviour given only by c_3 and c_{10}. The coefficients have long expressions, that cannot be reported. However, assuming beam properties of Table 1, $n = 1$ and $m = 2$, they are listed in Appendix C for twelve values of dimensionless spring stiffnesses $\kappa = \frac{k_s L}{EA}$. It is easy to see that c_1, c_2 and $c_6 - c_8$ are independent of κ, and that $c_3(\kappa = 0)$ is negative (softening), and becomes positive (hardening) for increasing κ. c_{10}, on the other end, is always positive, so that the second mode is always hardening, and for its largest value $c_{10}(\kappa = 1) = 7.3071 \times 10^6$ we are very close to a singularity (solutions escape to $\pm\infty$), see the nonlinear correction coefficient reported in [9]. However, it is still within the scope of our interest.

We eliminate exponential notation by introducing the real-valued functions $p_1(t_2)$, $q_1(t_2)$, $p_2(t_2)$ and $q_2(t_2)$:

$$A_1(t_2) = \frac{1}{2}\left(p_1(t_2) - iq_1(t_2)\right) e^{i\sigma_2 t_2}, \quad \bar{A}_1(t_2) = \frac{1}{2}\left(p_1(t_2) + iq_1(t_2)\right) e^{-i\sigma_2 t_2},$$

$$A_2(t_2) = \frac{1}{2}\left(p_2(t_2) - iq_2(t_2)\right) e^{i(3\sigma_2-\sigma_1)t_2}, \quad \bar{A}_2(t_2) = \frac{1}{2}\left(p_2(t_2) + iq_2(t_2)\right) e^{-i(3\sigma_2-\sigma_1)t_2}. \tag{53}$$

Grouping real and imaginary parts we get a set of four modulation equations:

$$\frac{\partial p_1(t_2)}{\partial t_2} = f_1 = -\sigma_2 q_1 + c_1 c_{U_I} p_1 + c_2 c_{\theta_I} p_1 + c_3\left(p_1^2 q_1 + q_1^3\right) + c_4\left(p_1^2(t_2)\, q_2 - 2p_2 p_1 q_1 - q_1^2 q_2\right) + c_5\left(p_2^2 q_1 + q_1 q_2^2\right), \tag{54}$$

$$\frac{\partial q_1(t_2)}{\partial t_2} = f_2 = \sigma_2 p_1 + c_1 c_{U_I} q_1 + c_2 c_{\theta_I} q_1 + c_3\left(-p_1 q_1^2 - p_1^3\right) + c_4\left(-2p_1 q_1 q_2 + p_2 q_1^2 - p_2 p_1^2\right) + c_5 p_1\left(-p_2^2 - q_2^2\right) - c_6 Q, \tag{55}$$

$$\frac{\partial p_2(t_2)}{\partial t_2} = f_3 = -(3\sigma_2 - \sigma_1) q_2 + c_7 c_{U_{II}} p_2 + c_8 c_{\theta_{II}} p_2 + c_9\left(p_1^2 q_2 + q_1^2 q_2\right) + c_{10}\left(p_2^2 q_2 + q_2^3\right) + c_{11}\left(3p_1^2 q_1 - q_1^3\right), \tag{56}$$

$$\frac{\partial q_2(t_2)}{\partial t_2} = f_4 = (3\sigma_2 - \sigma_1) p_2 + c_7 c_{U_{II}} q_2 + c_8 c_{\theta_{II}} q_2 + c_9\left(-p_2 q_1^2 - p_2 p_1^2\right) + c_{10}\left(-p_2 q_2^2 - p_2^3\right) + c_{11}\left(3p_1 q_1^2 - p_1^3\right). \tag{57}$$

The explicit dependence of p_1, q_1 and p_2, q_2 on t_2 is omitted to simplify the expressions.

The approximate solution (12) after substituting first (26)–(29), (30) and (43) takes the form:

$$\begin{aligned} W(Z,t) = \varepsilon^2 \frac{1}{2}\Big\{ & \frac{1}{2} W_{2a}(Z,n)(p_1^2 + q_1^2) + \frac{1}{2} W_{2b}(Z,n)(p_2^2 + q_2^2) \\ & + W_{2c}(Z,n)\left[(p_1^2 - q_1^2)\cos\left(2\omega_n t_0 + 2\sigma_2 t_2\right) + 2p_1 q_1 \sin\left(2\omega_n t_0 + 2\sigma_2 t_2\right)\right] \\ & + W_{2d}(Z,n)\left[(p_1^2 - q_1^2)\cos\left(-2\omega_m t_0 + 2\sigma_1 t_2 - 6\sigma_2 t_2\right) - 2p_1 q_1 \sin\left(-2\omega_m t_0 + 2\sigma_1 t_2 - 6\sigma_2 t_2\right)\right] \\ & + W_{2e}(Z,n)\left[(p_1 p_2 - q_1 q_2)\cos\left(-(\omega_n + \omega_m)t_0 + (\sigma_1 - 4\sigma_2)t_2\right) - (p_2 q_1 + p_1 q_2)\sin\left(-(\omega_n + \omega_m)t_0 + (\sigma_1 - 4\sigma_2)t_2\right)\right] \\ & + W_{2f}(Z,n)\left[(p_1 p_2 - q_1 q_2)\cos\left((-\omega_n + \omega_m)t_0 + (\sigma_1 - 4\sigma_2)t_2\right) - (p_2 q_1 + p_1 q_2)\sin\left((-\omega_n + \omega_m)t_0 + (\sigma_1 - 4\sigma_2)t_2\right)\right]\Big\} + \mathcal{O}(\varepsilon^3), \end{aligned} \tag{58}$$

$$\begin{aligned} U(Z,T) = \varepsilon\Big\{ & \left[p_1 \cos\left(\omega_n t_0 + \sigma_2 t_2\right) + q_1 \sin\left(\omega_n t_0 + \sigma_2 t_2\right)\right] \hat{U}_{1,n}(Z,n) \\ & + \left[p_2 \cos\left(-\omega_m t_0 + (\sigma_1 - 3\sigma_2)t_2\right) - q_2 \sin\left(-\omega_m t_0 + (\sigma_1 - 3\sigma_2)t_2\right)\right] \hat{U}_{1,m}(Z,n)\Big\} + \mathcal{O}(\varepsilon^3), \end{aligned} \tag{59}$$

$$\begin{aligned} \theta(Z,T) = \varepsilon\Big\{ & \left[p_1 \cos\left(t_0\omega_n + t_2\sigma_2\right) + q_1 \sin\left(\omega_n t_0 + \sigma_2 t_2\right)\right] \hat{\theta}_{1,n}(Z,n) \\ & + \left[p_2 \cos\left(-\omega_m t_0 + (\sigma_1 - 3\sigma_2)t_2\right) - q_2 \sin\left(-\omega_m t_0 + (\sigma_1 - 3\sigma_2)t_2\right)\right] \hat{\theta}_{1,m}(Z,n)\Big\} + \mathcal{O}(\varepsilon^3). \end{aligned} \tag{60}$$

Modulation Eqs. (54)–(57) enable investigation of amplitudes in the second slow time scale t_2 as well as frequency response curves of the simply supported beam with elastic boundary condition in the axial direction and nonlinear modal interactions between two successive flexural modes. The direct modal coupling is observed in Eq. (58) as products $p_1 p_2$, $q_1 q_2$, $p_2 q_1$ and $q_1 p_2$, while indirect modal coupling comes from the solution of Eqs. (54)–(57).

Commonly, only equilibria points of (54)–(57) are looked for, corresponding to stationary nonlinear oscillations of the original problem. Here, instead, we integrated (54)–(57) numerically, in order to highlight the presence of different kind of motions, like for example periodic solutions, corresponding to quasi-periodic motion of the physical system (an example is reported in forthcoming Fig. 4). More precisely, in Section 4 the brute force method is implemented to draw numerically stable solutions. These results are then compared with independent FE simulations. Next, the stability of the same frequency response curves for the steady state solutions is determined by studying the eigenvalues of the Jacobian matrix.

4. Results

Flexural–flexural interactions are of our interest as it is the natural extension of former works on uncoupled bending resonances. Thus, the dimensional mechanical properties of the structure, reported in Table 1, correspond to those used in [8,9,30,31,33,37]. Limiting the investigation only to the first two bending modes of the beam ($n = 1$, $m = 2$) the natural frequencies are $\omega_1 = 2899.52$ rad/s (461.47 Hz) and $\omega_2 = 11086.7$ rad/s (1764.5 Hz). It implies the first detuning parameter $\sigma_1 = \omega_2 - 3\omega_1 = 2388.14$ rad/s (380.28 Hz), which is 21% of ω_2, and the superharmonic resonance (i.e. $\Omega \approx \omega_2/3$) is expected at $\sigma_2 = \frac{1}{3}\omega_2 - \omega_1 = 796.05$ rad/s (126.76 Hz). Moreover, we assume constant amplitude of excitation $Q = 59839.5$ N. Except $c_{\theta_{II}}$, which is tuned to secondary branch (0.6%), the damping coefficients are adjusted to 6% of the natural modes: $c_{U_I} = 27.6883$ N s/m, $c_{\theta_I} = 4.51672$ N s/m, $c_{U_{II}} = 105.874$ N s/m, $c_{\theta_{II}} = 0.924837$ N s/m. Linear viscous damping coefficient of the second mode is fitted to the frequency response curve obtained from numerical simulations for $\kappa = 1$, and as a side-issue is not varied for different spring stiffnesses. We initially consider the force applied at a quarter of the length of the beam, $\bar{Z} = L/4$.

4.1. Brute force methods

Applying the brute force method with frequency sweep forward/backward to Eqs. (54)–(57), amplitudes $p_1(t_2)$, $q_1(t_2)$, $p_2(t_2)$, $q_2(t_2)$ are obtained by numerical integration in the slowest time scale t_2. For each fixed value of κ, the appropriate (one per each branch) initial conditions are chosen at $\sigma_2 = 1500$ rad/s; then, the frequency of excitation was gradually decreased step by step of about 1 rad/s, up to reaching $\sigma_2 = -500$ rad/s. This end the decreasing phase. Then, the frequency is increased, with the same step, up to reach again $\sigma_2 = 1500$ rad/s. With this approach we are able to detect the hysteresis loop to the nonlinear resonance, limiting to the stable solutions, even though we lose disconnected branches, like for example isolas. They will be detected analytically in the next section.

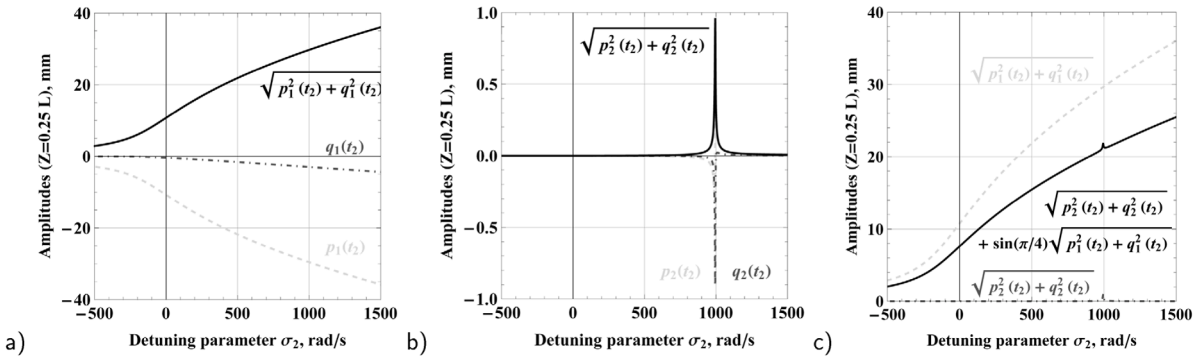

Fig. 2. Frequency response curve for sweep forward and $\kappa = 5$: amplitudes $p_1(t_2)$, $q_1(t_2)$ $p_2(t_2)$, $q_2(t_2)$ and maximum amplitudes for the first (a) and second (b) modes — solid black lines. Two-mode equilibrium solution at $Z = 1/4L$ - solid black line (c).

An example of resultant amplitude for first and second vibration modes are displayed in Fig. 2a,b. To illustrate the behaviour of the beam due to both involved modes, i.e to highlight the effect of the nonlinear coupling due to the internal resonance, we select a given point and report the amplitude of its transversal displacement. We choose the same point where the force is applied. For $Z = L/4$, the first mode has multiplier $\sin(\pi/4) = 0.707107$, while the second mode is taken into account as the maximum value and the gain is equal to $\sin(\pi/2) = 1$. The resultant amplitude for the motion of this point is presented in Fig. 2c.

In Fig. 3 the results of Fig. 2c are extended to different values of κ, and compared with FE solutions. For detailed information on the FE model we refer to our previous works [8,12,30,33,37]. An overall very good agreement between theoretical and FE solutions is found (at least for moderate amplitude, where the asymptotic solutions is expected to be valid), thus confirming the reliability of the former.

For $\kappa = 0$ the system is softening (the curve bends towards the left), and no modal interaction is observed. By slightly increasing κ, up to 0.1, we move to an hardening behaviour (the transition for softening to hardening is when $c_3 = 0$, i.e. at $\kappa \approx 0.018$, see Appendix C). Furthermore, and more important for the scope of this work, the modal coupling clearly appears as the extra peak of the main resonant (upper) branch, which is also hardening, according to the fact that the second mode is hardening, too. It looks like as a (secondary) resonance on top of another (principal) resonance. This happens at $\sigma_2 \approx 700$, i.e. when $\Omega \approx \omega_2/3$, showing that it is activated by the internal resonance. In fact, we remind that, at least in the analytical computations, the second mode is not directly forced (in (47)–(48) there is no excitation in the terms multiplying $e^{i\omega_m t_0}$; and no excitation in (56)–(57), too).

For the previous value of κ the modal coupling has the largest effect. By further increasing κ, the extra peak due to internal resonance decreases its amplitude, and occurs for increasing values of the forcing frequency, however always in the neighbourhood of $\Omega \approx \omega_2/3$, i.e. in a neighbourhood of $\sigma_2 = 796.05$. Simultaneously, the main frequency response curve is more and more bent, according to the fact that c_3 (strongly) increases with κ (see Appendix C). For large value of κ, say for $\kappa > 10$, the extra peak practically disappears, and the modal coupling has no more effects on the main resonance curve of the first mode.

Noticeable effects of the modal coupling appear only for the upper (resonant) stable solutions, while the bottom (non resonant) solutions seem to be smooth and undisturbed.

The solutions along the various branches of Fig. 3 are fixed points of (54)–(57), i.e. periodic solutions of the physical system. However, for $\kappa = 0.25$, $\kappa = 0.5$, $\kappa = 1$ and $\kappa = 3$, see Fig. 3c–f, there are other solutions, in particular periodic one, corresponding to quasi-periodic motion of the physical system. This is highlighted by the red circle in Fig. 3e. In FE simulations similar phenomenon is observed only for $\kappa = 3$. These very narrow ranges may be overlooked by too rare sampling of frequency excitation (25 rad/s) or when the stability of this non equilibrium solution is lost and consequently the solution escapes to a different stable branch. Zoom of the secondary resonance for $\kappa = 1$ and corresponding time histories of the points marked with circles of Fig. 3e are illustrated in Fig. 4. It is seen that, after an initial transient, two solutions (for $\sigma = 1050$ rad/s (upper branch, green) and $\sigma = 1200$ rad/s (blue)) approach a constant value, in contrast to red solution that converges to a periodic motion.

Let us investigate the peak detected in the FE simulations for $\kappa = 3$ and $\sigma_2 = 1075.48$ rad/s ($\Omega = 3975$ rad/s), corresponding to a solution with the very high period $P \approx 0.031$ s (that is 20 times the period of the excitation $2\pi/3975 = 0.00158$ s), see Fig. 5. An internal resonance induced periodic energy exchange between the axial and transversal motion is observed in Fig. 5a. When the amplitude in the transverse direction significantly decreases, the largest value of $W(Z = L)$ becomes positive, which corresponds to dynamic beam stretching. The longitudinal vibrations are proportional to the transverse movement and after one period the energy transfer is repeated again. In parallel, the fast Fourier transform was performed to find the desired natural frequencies, in which integer ratios of the frequency of excitation (Ω), first two flexural (ω_{01} and ω_{02}) modes and the first longitudinal ($\omega_{A01} = 26644,78$ Hz) mode were included, see Fig. 5b. Generally, linear analysis is ineffective due to large amplitudes of vibrations in lateral direction, which causes nonlinearities also in the longitudinal direction, so that the following conclusions are only preliminary. In addition to the closeness of ω_{02} and 3Ω, which is lurking in the background (see the previous analysis), we also observe that around the first peak of the transversal motion U (grey) we have $\Omega \approx \omega_{A01}/6$, i.e. a 6:1 superharmonic resonance with the longitudinal mode, while around the first peak in the longitudinal direction (black) we have $2\Omega \approx \omega_{A01}/3$. The closer examination of this case, that likely involve a very challenging 6 to 2 to 1 flexural–flexural–longitudinal internal resonances of Timoshenko beams, is left for future works.

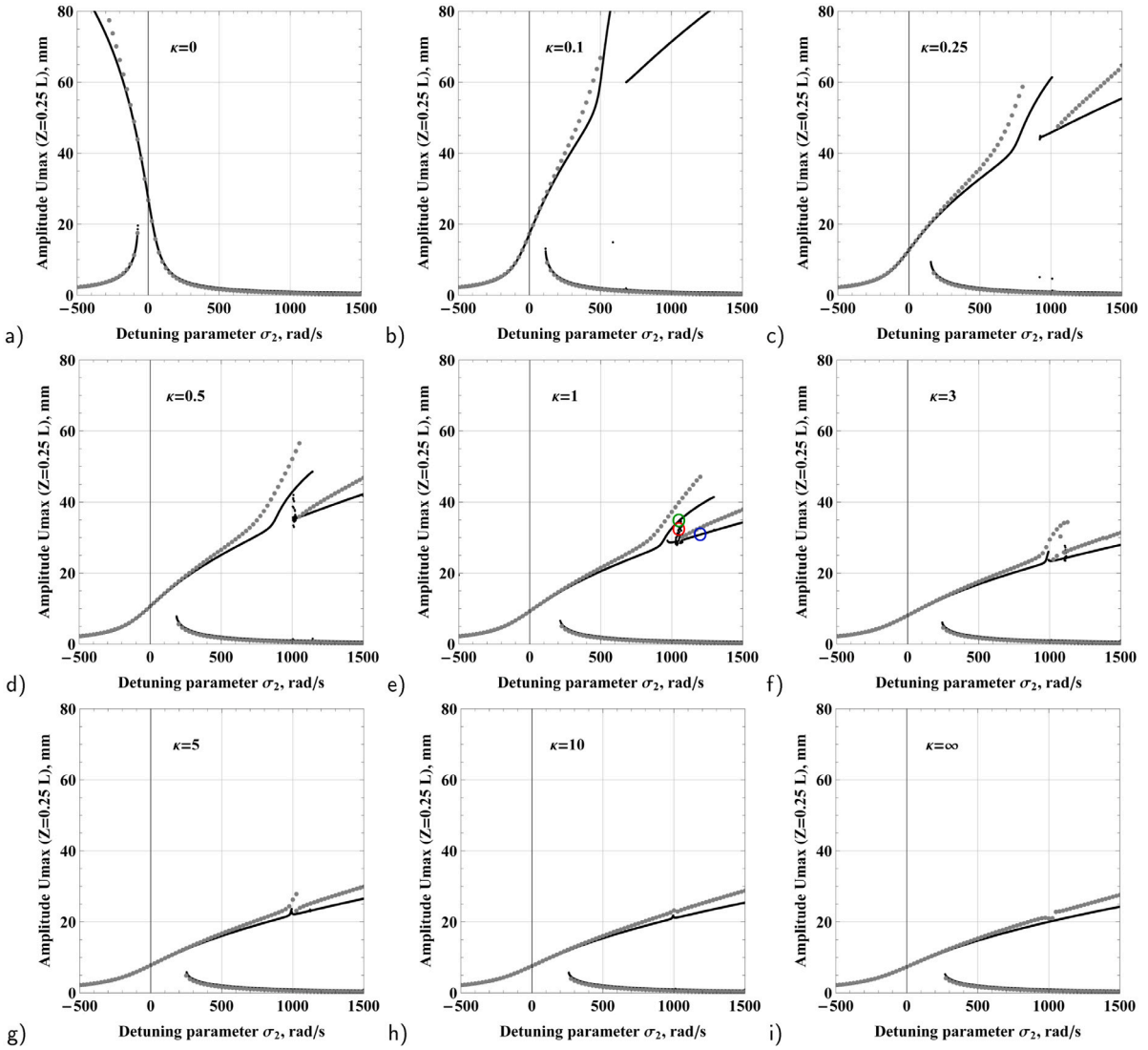

Fig. 3. Frequency response curves obtained by brute force methods for various spring stiffens $[0, +\infty)$ of the beam: grey dots — FEM, black dots MTSM. (For interpretation of the references to colour in this figure legend, the reader is referred to the web version of this article.)

4.2. Isolas detection and stability analysis

It is a very demanding task to grab all solutions of (54)–(57), which carries the risk of overlooking certain solutions of the four-dimensional space, in particular unexpected isolas, in spite of the fact that techniques for the construction of basins of attraction have been improved over the years [38,39]. To relieve such problem we consider the equilibrium points of the ordinary differential Eqs. (54)–(57), i.e. $f_1 = f_2 = f_3 = f_4 = 0$, that then become four fully nonlinear and fully coupled but algebraic equations, that thus can be "fully" solved for each frequency of excitation σ_2. Full frequency response curves are gathered in Fig. 6.

Next, the stability of the reported solutions is determined by the eigenvalues of the Jacobian matrix:

$$J = \begin{bmatrix} \frac{\partial f_1}{\partial p_1} & \frac{\partial f_1}{\partial q_1} & \frac{\partial f_1}{\partial p_2} & \frac{\partial f_1}{\partial q_2} \\ \frac{\partial f_2}{\partial p_1} & \frac{\partial f_2}{\partial q_1} & \frac{\partial f_2}{\partial p_2} & \frac{\partial f_2}{\partial q_2} \\ \frac{\partial f_3}{\partial p_1} & \frac{\partial f_3}{\partial q_1} & \frac{\partial f_3}{\partial p_2} & \frac{\partial f_3}{\partial q_2} \\ \frac{\partial f_4}{\partial p_1} & \frac{\partial f_4}{\partial q_1} & \frac{\partial f_4}{\partial p_2} & \frac{\partial f_4}{\partial q_2} \end{bmatrix}, \quad \text{Eigenvalues } [J] = \{x_1 + iy_1, x_2 + iy_2, x_3 + iy_3, x_4 + iy_4\}. \tag{61}$$

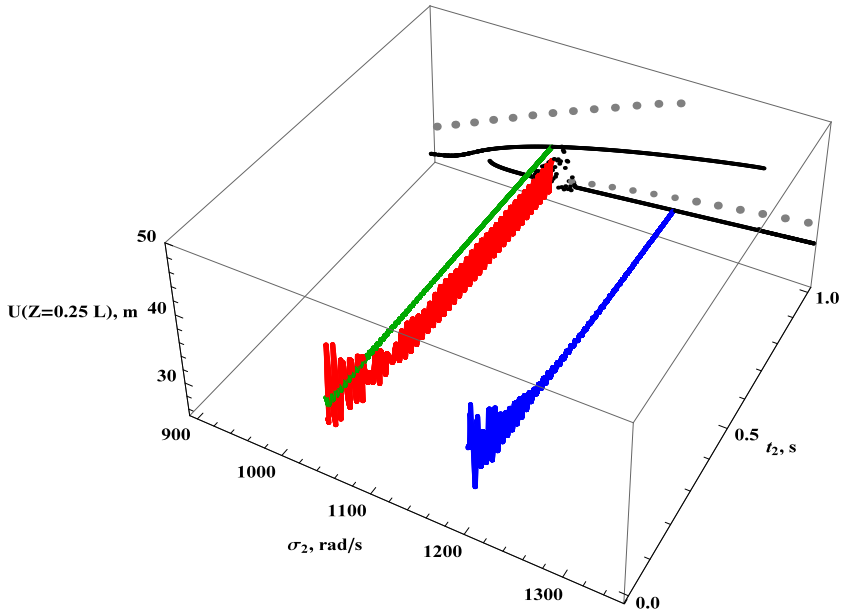

Fig. 4. Zoom of frequency response curves obtained by brute force methods by FEM (grey) and MTSM (black) for $\kappa = 1$. Selected time histories in the slow time scale t_2 (MTSM): green and blue — fixed points, red — the limit cycle. (For interpretation of the references to colour in this figure legend, the reader is referred to the web version of this article.)

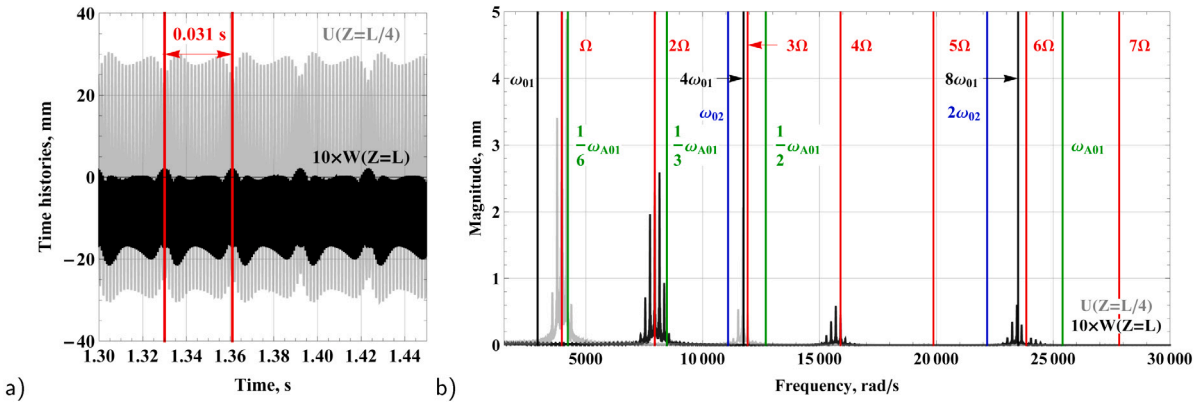

Fig. 5. Time histories from FE simulations for $\kappa = 3$, $\Omega = 3975$ rad/s ($\sigma_2 = 1075.48$ rad/s) (a) and their fast Fourier transform (b). (For interpretation of the references to colour in this figure legend, the reader is referred to the web version of this article.)

The solution is stable when all eigenvalues have negative real part, while the solution is unstable if at least one real part is positive. The system of four differential equations has a much greater number of instability scenarios comparing to a two-dimensional systems, nevertheless, in this work we observe only two general instabilities: a saddle-type solution, for a real positive eigenvalue, and source-type solution, for complex eigenvalue with positive real part:

$$\text{if } \left(x_1 > 0 \bigwedge y_1 = 0\right) \vee \left(x_2 > 0 \bigwedge y_2 = 0\right) \vee \left(x_3 > 0 \bigwedge y_3 = 0\right) \vee \left(x_4 > 0 \bigwedge y_4 = 0\right) \rightarrow \text{unstable saddle-type},$$
$$\text{if } \left(x_1 > 0 \bigwedge y_1 \neq 0\right) \vee \left(x_2 > 0 \bigwedge y_2 \neq 0\right) \vee \left(x_3 > 0 \bigwedge y_3 \neq 0\right) \vee \left(x_4 > 0 \bigwedge y_4 \neq 0\right) \rightarrow \text{unstable source-type},$$
$$\text{if } x_1 < 0 \wedge x_2 < 0 \wedge x_3 < 0 \wedge x_4 < 0 \rightarrow \text{stable}.$$

Worth noting is the detached, partially-stable solution path presented in Fig. 6a, which shows three stability scenarios. Due to the huge amplitude of vibrations and small basin of attraction its stable branch was not detected in FE simulations, not even using a very accurate shooting procedure. Source-type instabilities appear only at higher amplitude branches for $\kappa \leq 5$, their centre moves with the spring stiffness and the largest green interval corresponds to $\kappa = 0.5$.

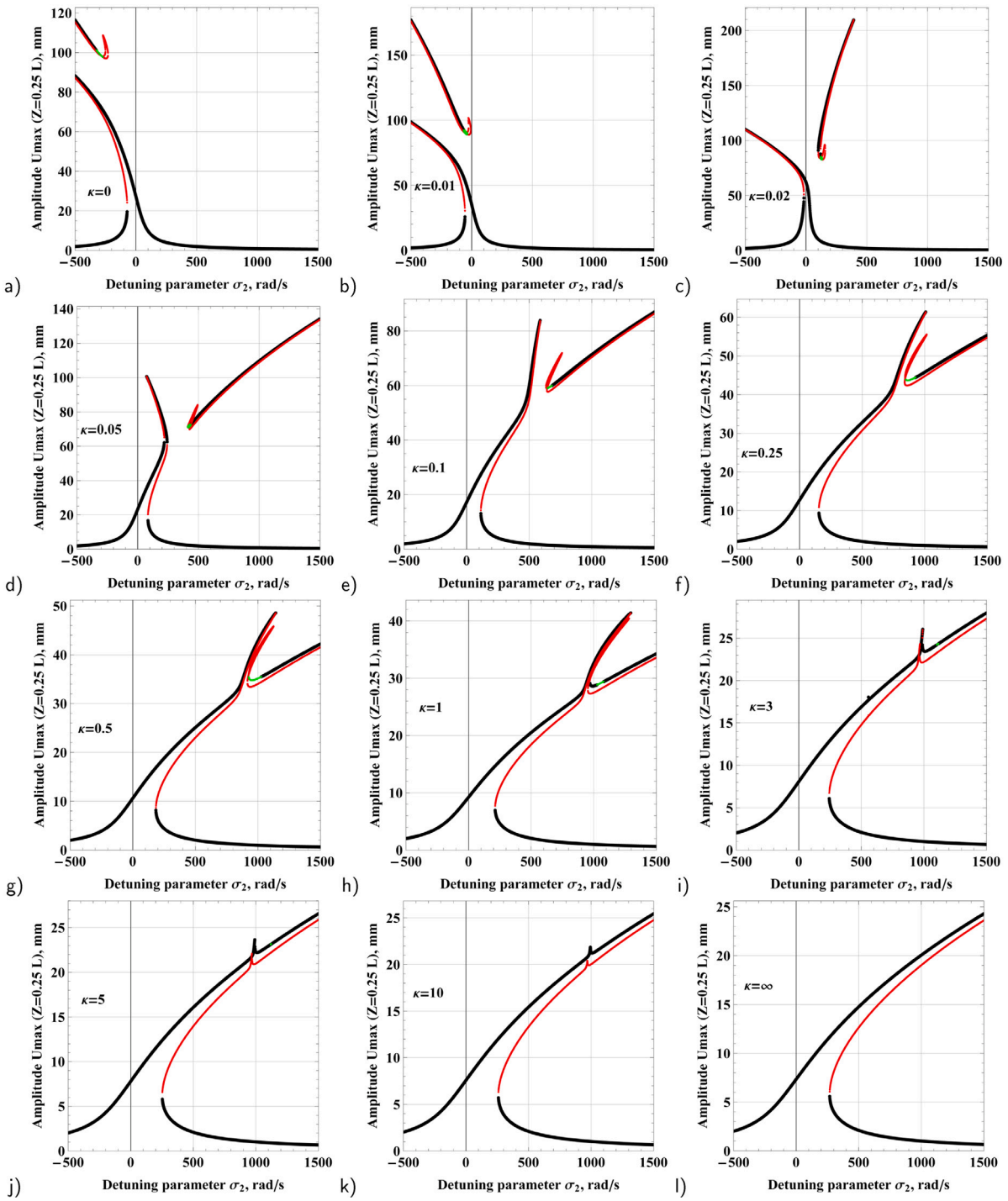

Fig. 6. Stability analysis of algebraic equations (54)–(57) for $f_1 = f_2 = f_3 = f_4 = 0$, black (green and red) denotes stable (unstable source-type and saddle-type) paths. (For interpretation of the references to colour in this figure legend, the reader is referred to the web version of this article.)

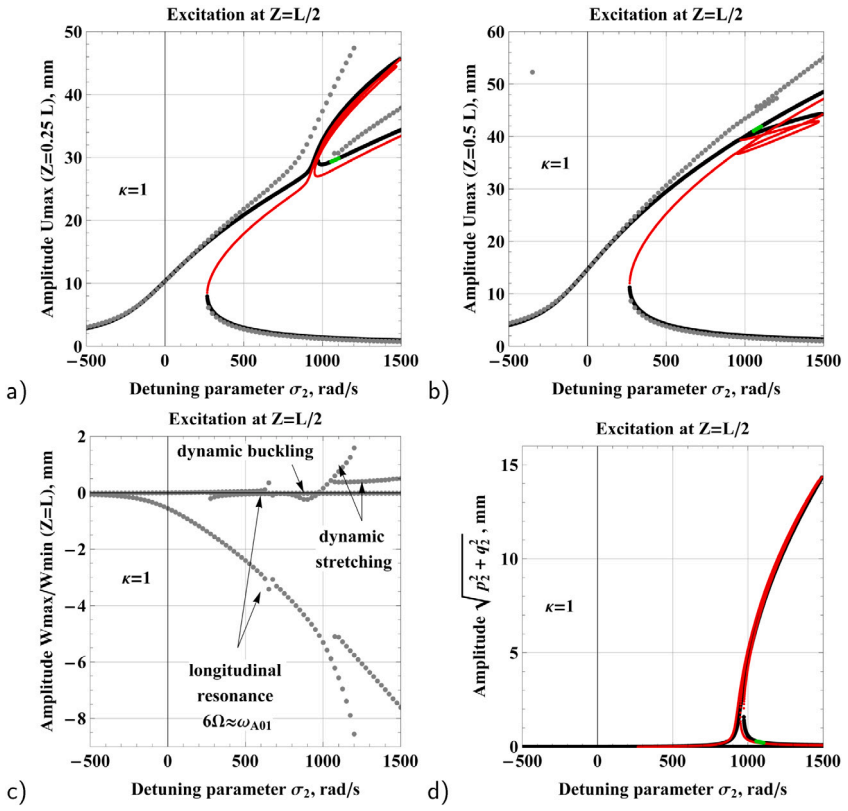

Fig. 7. Frequency response curves for external load at $\bar{Z} = L/2$, grey (black, red and green) dots are results obtained in FEM (MTSM): transversal displacement at $Z = l/4$ (a) transversal displacement at $Z = L/2$ (b) maximum and minimum of the longitudinal motion (only FE simulations) (c) and amplitude of the second mode (only MTSM) (d). (For interpretation of the references to colour in this figure legend, the reader is referred to the web version of this article.)

Large amplitude solutions for $\kappa = 0.01$, $\kappa = 0.02$, $\kappa = 0.05$, $\kappa = 0.1$, and $\kappa = 0.25$ are also separated from principal resonance (isola), see Fig. 6b-f. In all investigated cases, the nonlinear response of the first bending mode is disturbed only by activating the secondary resonance, but passing this area, the dynamic couplings disappear and return to the first mode alone. The secondary responses bend towards right for $\kappa \geq 0.1$, while axial boundary condition of lower stiffness generates slope of the curve to the left. We assume that observed mechanism is affected by significant longitudinal movement, similarly to the first flexural mode of simply supported beam ($\kappa = 0$), in which the axial inertia terms soften the primary resonance curve. Fig. 6d attracts particular attention with transition from hardening of primary response to softening of secondary response giving us full control over the system. The interval 588 rad/s $\leq \sigma_2 \leq$ 683 rad/s of $\kappa = 0.1$ shows only one stable branch and explains absence of second stable branch in Fig. 3e. This result has been cross checked in laborious brute force and shooting initial conditions methods by FE simulations for $\kappa = 0.125$ as well as $\kappa = 0.25$ in [31], and implicitly proves the correctness of the analytical model.

4.3. Internal resonance mechanism

We transfer the concentrated load from $\bar{Z} = L/4$ to $\bar{Z} = L/2$ in the numerical and analytical studies to further confirm that the modal coupling is due to internal resonance 3:1 and not to a 3:1 superharmonic resonance. Now, the external load is imposed at the modal node of the second flexural mode, thus it is no longer directly excited by the concentrated force, not even in the FE simulations.

Comparison between numerical and analytical outcomes are presented for $\kappa = 1$ in Fig. 7. Overall, MTSM and FE results fit together very well, also in terms of bifurcation frequencies and unstable intervals. However, the numerical and analytical results *quantitatively* differ more and more as the detuning parameter σ_2 increases, or better as the amplitude of the motion increases, as expected due to the perturbative nature of the solution (but the *qualitative* similitude is maintained in any case). Certainly the higher orders analytical approximations will give better quantitative agreement with numerical simulations. The side issue can be also related to the frequency-dependent damping coefficient in Abaqus_CAE© software.

At first glance, dynamical behaviour of the beam–spring system ($\kappa = 1$) for excitation at the beam midpoint displayed in Fig. 7a does not differ from dynamical response presented in Fig. 3e (note that there are different vertical scales in the two figures). The main difference is that the secondary resonant stable branch is even better highlighted. Moreover, the unstable source-type area is slightly

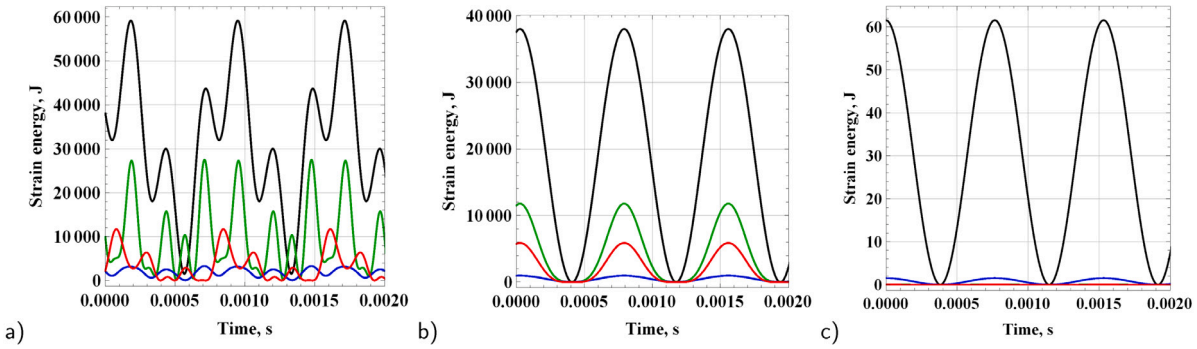

Fig. 8. Time histories of strain energies in bending (black), elongation (green), shear (blue) deformability of the beam and in the axial spring (red): the highest (a), intermediate (b) and lowest (c) amplitudes of steady state oscillations. Case $\sigma_2 = 1200$ rad/s of Fig. 7a. (For interpretation of the references to colour in this figure legend, the reader is referred to the web version of this article.)

shifted towards higher frequencies, and the agreement of numerical and analytical results is the same. The modal decomposition into the basic transverse modes, together with the fact that the second mode has a node at $Z = L/2$, is at the base of the fact that the transversal displacement at $Z = L/2$ does not have the extra peak due to modal coupling, both in analytical and FE simulations (Fig. 7b). The contribution of the second mode is shown in Fig. 7d.

Very interesting FE results are observed for the longitudinal dynamic response of the beams tip, see Fig. 7c. Starting from the lowest frequency of excitation $\sigma_2 = -500$ rad/s, the pulsating axial oscillations have a maximum displacement that is negligible, while the minimum displacement (and thus its overall amplitude) increases almost like a parabola. The first relevant phenomena appears for about $\sigma_2 = 650$ rad/s (i.e. at $\Omega = 3549.52$ rad/s). Considering that the first natural frequency in the axial direction is $\omega_{A01}(\kappa = 1) = 20\,985.84$ rad/s, it can be found that $\frac{1}{6}\omega_{A01}(\kappa = 1) = 3497.64 \approx \Omega$ rad/s, i.e. we are close to 6:1 superharmonic resonance of the axial mode (see Fig. 5 where this phenomenon is also illustrated). The born of the secondary flexural resonance is credited at 900 rad/s and it activates dynamic buckling of the beam. In the other words, the tip of the beam does not return to its initial position and the first flexural mode indirectly by the longitudinal motion activates the second and higher order flexural modes as well. Passing the dynamic buckling zone, at $\sigma_2 = 975$ rad/s, we move to a zone with axial dynamic stretching correlated with large amplitudes of both fundamental and secondary responses.

To better understand the various relative contributions to the beam motion, let us compute (up to the second order) the flexural, axial and shear strain energies, as well as the strain energy of the boundary spring. For this purpose we choose three stable branches at $\sigma_2 = 1200$ rad/s of Fig. 7a, (i) the highest, $U_{max} = 39.4674$ mm involving the fundamental and secondary response, (ii) the intermediate, $U_{max} = 31.0515$ mm due only to the fundamental resonance, and (iii) the lowest, $U_{max} = 1.23173$ mm related to the non resonant branch (Fig. 8). As expected, the largest strain energy is accumulated in the highest vibration amplitude, wherein the maximum strain energy due to elongation/compression is about one half of the bending strain energy: this proves how the axial deformability cannot be neglected, and that the axial motion is very influential as a "carrier" between flexural modes. On the other hand, the maximum energy contained in the spring is slightly lesser than one half of strain energy due to elongation of the beam, showing how it plays a minor, but not negligible, role. Furthermore, an energy transfer mechanism between the beam and the spring exists, since as one increases, the other decreases. The energy due to shearing effect may be attributed rather to fast oscillations of the second flexural mode than to slow oscillations of first bending mode, according to the fact that higher order modes are more prone to shear deformation. When secondary response is not activated, the fundamental resonance becomes smooth and have only one harmonic ΩT, and contribution of the shearing effect reduces (Fig. 8b). We note that energy of the axial spring and beam's axial deformations are still significant, see Fig. 8b. Finally, for small oscillations the axial spring and the extensibility of the beam become negligible, according to the fact that the solution approaches the linear problem and nonlinear longitudinal–transversal couplings do not occur). On the contrary, the shear strain energy does not reduce its magnitude (while remaining in any case small, i.e. about 2.5% of the flexural energy).

5. Conclusions and final remarks

Nonlinear dynamics of the hinged–simply supported extensible shearable beam with an axial spring have been studied in the paper in a neighbourhood of an internal resonance between two transversal modes. First, perturbation method have been applied to the problem to derive modulation equations, which capture flexural–flexural nonlinear modal interactions, that occurs also by the involvement of the axial motions. It is shown that the increase of the axial spring stiffness changes the hardening/softening behaviour of the first flexural mode, moreover affects the secondary resonance (due to the internal resonance) localization and amplitude. Stable, unstable saddle-type and unstable source-type solutions have been observed by Jacobi stability analysis. Secondly, results of analytical and numerical approaches have been confronted with a very good agreement. Raised reliability of the problem prelude the future experimental validation.

For the initially straight beams the dynamic coupling between flexural modes is often neglected, which explains little knowledge on this topic in the literature. The vast majority of the research done has been limited only to beams with buckling, axial loading or pre-deflection. On the basis of the calculations performed by two independent methods, the interactions between the two modes were carefully tested. In the future work authors plan to investigate the condition of longitudinal deformation in the first order of the approximate solution $W_1(Z,T) \neq 0$ as well as the more rigorous condition of the transverse–transverse–longitudinal internal resonance which is a heavy task to be done analytically, and to date can be done only by the FE method.

On the basis of the presented results, we conclude that taking into account in the analytical model the dynamics in the longitudinal direction is very important for the appearance of axially-induced 3:1 flexural internal resonance. This argument is strengthened by the lack of this phenomenon for the fixed- fixed beam, where the axial displacement is null by the constraint, at least at the boundaries (see Figs. 3i and 6i).

The considered Timoshenko beam model takes into account the shearing effect and inertia from rotation of cross-section, which for the sake of simplification could by omitted, but improves the accuracy of the results and enables investigation the interactions of higher flexural and longitudinal modes (e.g. ω_{03}, ω_{04} and ω_{A02}).

CRediT authorship contribution statement

Lukasz Kloda: Conceptualization, Methodology, Software, Validation, Formal analysis, Data curation, Writing – original draft, Writing – review & editing. **Stefano Lenci:** Conceptualization, Writing – review & editing, Supervision. **Jerzy Warminski:** Writing – review & editing, Supervision. **Zofia Szmit:** Writing – review & editing.

Declaration of competing interest

The authors declare that they have no known competing financial interests or personal relationships that could have appeared to influence the work reported in this paper.

Acknowledgement

The work is financially supported by grant 2019/33/N/ST8/02661 from the National Science Centre, Poland.

Appendix A

$$f_1(l) = -\left(EI^2\pi^2 - 2L^2\rho\omega_l^2\right)\frac{2l\pi Z + L(\kappa+1)\sin\left(\frac{2l\pi Z}{L}\right)}{4EL^2l\pi\left(k_s+1\right)}, \quad l \in \mathbb{N}_+, \quad \kappa = \frac{k_s L}{EA},$$
$$W_{2a}(Z) = f_1(l=n), \quad W_{2b}(Z) = f_1(l=m), \tag{A.1}$$
$$f_2(l) = \frac{(EI^2\pi^2 - 2L^2\rho\omega_l^2)}{16L^2(-EI^2\pi^2 + L^2\rho\omega_l^2)\left[\sqrt{E}A\sqrt{\rho}\omega_l\cos\left(\frac{2L\sqrt{\rho}\omega_l}{\sqrt{E}}\right) + k_s\sin\left(\frac{2L\sqrt{\rho}\omega_l}{\sqrt{E}}\right)\right]}$$
$$\times\left\{\pi Ll\sin\left(\frac{2\pi lZ}{L}\right)\left[2\sqrt{E}A\sqrt{\rho}\omega_l\cos\left(\frac{2L\sqrt{\rho}\omega_l}{\sqrt{E}}\right) + k_s\sin\left(\frac{2L\sqrt{\rho}\omega_l}{\sqrt{E}}\right)\right]\right.$$
$$\left. - \sin\left(\frac{2\sqrt{\rho}Z\omega_l}{\sqrt{E}}\right)\left[2AL^2\rho\cos(2\pi l)\omega_l^2 + 2AL^2\rho\omega_l^2 - 2E\pi^2Al^2 + \pi k_s Ll\sin(2\pi l)\right]\right\}, \quad l \in \mathbb{N}_+,$$
$$W_{2c}(Z) = f_2(l=n), \quad W_{2d}(Z) = f_2(l=m). \tag{A.2}$$

The functions $W_{2e}(Z)$ and $W_{2f}(Z)$ have very long expressions. They can be detected by the symbolic software Mathematica© we used for the computations, but cannot be reported here. For fixed parameters of Table 1 they are given by:

$$W_{2e} = \frac{1}{k_s + 3.16\times10^8}\times\left\{(32.65k_s - 6.05\times10^{10})\sin(2.70Z) - (9.72k_s + 3.06\times10^9)\sin(6.28Z)\right.$$
$$-(1.84k_s + 5.82\times10^8)\sin(18.84Z) - (26.19k_s + 8.262\times10^9)\cos(2.70Z)$$
$$\left.+(k_s + 3.15\times10^8)[28.86\cos(6.28Z) - 2.67\cos(18.85Z)]\right\}, \tag{A.3}$$
$$W_{2f} = \frac{-8.86\times10^{10}\sin(1.58Z) + 2.86\times10^{-6}\sin(6.28Z) - 4.77\times10^{-7}\sin(18.85Z)}{k_s + 8.21\times10^8} + 53.80\sin(1.58Z)$$
$$-\ 8.46\sin(6.28Z) - 1.82171\sin(18.85Z) - 22.48\cos(1.58Z) + 25.11\cos(6.28Z) - 2.63\cos(18.85Z). \tag{A.4}$$

Appendix B

All next functions depend on the space variable Z, which is omitted to simplify the notation.

$$
\begin{aligned}
U_{3a} &= EA\left(U'_{1,n}W'_{2a} + U'_{1,n}W'_{2c} + \frac{3}{2}U'^{3}_{1,n}\right)' + AG\left(U'_{1,n}W'_{2a} + U'_{1,n}W'_{2c} - \frac{3}{2}\theta_{1,n}U'^{2}_{1,n} + \frac{5}{2}U'^{3}_{1,n}\right)',\\
U_{3b} &= EA\left(3U'_{1,n}U'^{2}_{1,m} + U'_{1,n}W'_{2b} + U'_{1,m}W'_{2e} + U'_{1,m}W'_{2f}\right)'\\
&\quad + AG\left(-2\theta_{1,m}U'_{1,n}U'_{1,m} + 5U'_{1,n}U'^{2}_{1,m} + U'_{1,n}W'_{2b} + U'_{1,m}W'_{2e} + U'_{1,m}W'_{2f} - \theta_{1,n}U'^{2}_{1,m}\right)',\\
U_{3c} &= EA\left(\frac{3}{2}U'^{2}_{1,n}U'_{1,m} + U'_{1,n}W'_{2f} + U'_{1,m}W'_{2c}\right)' + AG\left(-\theta_{1,n}U'_{1,n}U'_{1,m} + \frac{5}{2}U'^{2}_{1,n}U'_{1,m} + U'_{1,n}W'_{2f} - \frac{1}{2}\theta_{1,m}U'^{2}_{1,n} + U'_{1,m}W'_{2c}\right)',\\
U_{3d} &= EA\left(3U'^{2}_{1,n}U'_{1,m} + U'_{1,n}W'_{2e} + U'_{1,n}W'_{2f} + U'_{1,m}W'_{2a}\right)'\\
&\quad + AG\left(-2\theta_{1,n}U'_{1,n}U'_{1,m} + 5U'^{2}_{1,n}U'_{1,m} + U'_{1,n}W'_{2e} + U'_{1,n}W'_{2f} - \theta_{1,m}U'^{2}_{1,n} + U'_{1,m}W'_{2a}\right)',\\
U_{3e} &= EA\left(U'_{1,m}W'_{2b} + U'_{1,m}W'_{2d} + \frac{3}{2}U'^{3}_{1,m}\right)' + AG\left(U'_{1,m}W'_{2b} + U'_{1,m}W'_{2d} - \frac{3}{2}\theta_{1,m}U'^{2}_{1,m} + \frac{5}{2}U'^{3}_{1,m}\right)',\\
U_{3f} &= EA\left(U'_{1,n}W'_{2c} + \frac{1}{2}U'^{3}_{1,n}\right)' + AG\left(U'_{1,n}W'_{2c} - \frac{1}{2}\theta_{1,n}U'^{2}_{1,n} + \frac{5}{6}U'^{3}_{1,n}\right)',
\end{aligned}
\tag{B.1}
$$

$$
\begin{aligned}
\theta_{3a} &= EJ\left(\frac{3}{2}U'^{2}_{1,n}\theta'_{1,n} + W'_{2a}\theta'_{1,n} + W'_{2c}\theta'_{1,n}\right)' + AG\left(\frac{3}{2}\theta_{1,n}U'^{2}_{1,n} - \frac{1}{2}U'^{3}_{1,n} + \theta_{1,n}W'_{2a} + \theta_{1,n}W'_{2c}\right),\\
\theta_{3b} &= EJ\left(2U'_{1,n}U'_{1,m}\theta'_{1,m} + U'^{2}_{1,m}\theta'_{1,n} + W'_{2b}\theta'_{1,n} + W'_{2e}\theta'_{1,m} + W'_{2f}\theta'_{1,m}\right)'\\
&\quad + AG\left(2\theta_{1,m}U'_{1,n}U'_{1,m} - U'_{1,n}U'^{2}_{1,m} + \theta_{1,n}U'^{2}_{1,m} + \theta_{1,n}W'_{2b} + \theta_{1,m}W'_{2e} + \theta_{1,m}W'_{2f}\right),\\
\theta_{3c} &= EJ\left(U'_{1,n}U'_{1,m}\theta'_{1,n} + \frac{1}{2}U'^{2}_{1,n}\theta'_{1,m} + W'_{2c}\theta'_{1,m} + W'_{2f}\theta'_{1,n}\right)'\\
&\quad + AG\left(\theta_{1,n}U'_{1,n}U'_{1,m} - \frac{1}{2}U'^{2}_{1,n}U'_{1,m} + \frac{1}{2}\theta_{1,m}U'^{2}_{1,n} + \theta_{1,m}W'_{2c} + \theta_{1,n}W'_{2f}\right),\\
\theta_{3d} &= EJ\left(2U'_{1,n}U'_{1,m}\theta'_{1,n} + U'^{2}_{1,n}\theta'_{1,m} + W'_{2a}\theta'_{1,m} + W'_{2e}\theta'_{1,n} + W'_{2f}\theta'_{1,n}\right)'\\
&\quad + AG\left(2\theta_{1,n}U'_{1,n}U'_{1,m} - U'^{2}_{1,n}U'_{1,m} + \theta_{1,m}U'^{2}_{1,n} + \theta_{1,m}W'_{2a} + \theta_{1,n}W'_{2e} + \theta_{1,n}W'_{2f}\right),\\
\theta_{3e} &= EJ\left(\frac{3}{2}U'^{2}_{1,m}\theta'_{1,m} + W'_{2b}\theta'_{1,m} + W'_{2d}\theta'_{1,m}\right)' + AG\left(\frac{3}{2}\theta_{1,m}U'^{2}_{1,m} - \frac{1}{2}U'^{3}_{1,m} + \theta_{1,m}W'_{2b} + \theta_{1,m}W'_{2d}\right),\\
\theta_{3f} &= EJ\left(\frac{1}{2}U'^{2}_{1,n}\theta'_{1,n} + W'_{2c}\theta'_{1,n}\right)' + AG\left(\frac{1}{2}\theta_{1,n}U'^{2}_{1,n} - \frac{1}{6}U'^{3}_{1,n} + \theta_{1,n}W'_{2c}\right).
\end{aligned}
\tag{B.2}
$$

Appendix C

In this section we report the values of the parameters c_i for increasing stiffness of the axial spring, when $n = 1$, $m = 2$, $A = 0.05 \times 0.05$ m^2, $L = 0.5$ m, $E = 210$ GPa, $G = 68.6538$ GPa, $\rho = 7580$ kg m^{-3}.

$\kappa = \frac{k_s L}{EA}$	0	0.01	0.02	0.05	0.1	0.25
c_1	−0.025280	−0.025280	−0.025280	−0.025280	−0.0252780	−0.0252780
c_2	−0.949995	−0.949995	−0.949995	−0.949995	−0.949995	−0.949995
c_3	−24651.43	−10939.91	2490.74	41 181.43	100 784.26	249 971.76
c_4	−191777.1	−189407.84	−187096.58	−180489.98	−170460.02	−146110.99
c_5	−972637.75	−918258.89	−865873.37	−719332.32	−504281.06	−6270.2992
c_6	2.466×10^{-5}	2.466×10^{-5}	2.466×10^{-5}	2.466×10^{-5}	2.466×10^{-5}	2.466×10^{-5}
c_7	−0.024801	−0.024801	−0.024801	−0.024801	−0.024801	−0.024801
c_8	−3.250212	−3.250212	−3.250212	−3.250212	−3.250212	−3.250212
c_9	−249496.4	−235700.2	−222412.2	−185254.2	−130758.5	−4697.221
c_{10}	2.9183×10^6	2.9574×10^6	2.9961×10^6	3.10916×10^6	3.28947×10^6	3.787731×10^6
c_{11}	−2540.930	−2512.790	−2485.267	−2406.201	−2285.041	−1985.162

$\kappa = \frac{k_s L}{EA}$	0.5	1	3	5	10	∞
c_1	−0.025280	−0.025280	−0.025280	−0.025280	−0.025280	−0.0252780
c_2	−0.949995	−0.949995	−0.949995	−0.949995	−0.949995	−0.949995
c_3	430 409.8	653 150.8	981 769.1	1.089924×10^6	1.187671×10^6	1.304253×10^6
c_4	−118026.8	−85265.42	−40414.8	−26485.59	−14227.38	−1.537064
c_5	548 918.7	1.1965×10^6	2.1159×10^6	2.413956×10^6	2.6824×10^6	3.0018×10^6
c_6	2.466×10^{-5}	2.466×10^{-5}	2.466×10^{-5}	2.466×10^{-5}	2.466×10^{-5}	2.466×10^{-5}
c_7	−0.024801	−0.024801	−0.024801	−0.024801	−0.024801	−0.024801
c_8	−3.250216	−3.250216	−3.250216	−3.250216	−3.250216	−3.250216
c_9	135 653.9	299 175.2	531 147.6	606 316.5	673 999.2	754 530.5
c_{10}	4.5807×10^6	7.3071×10^6	3.29765×10^6	4.0686×10^6	4.5463×10^6	5.0060×10^6
c_{11}	−1628.88	−1198.64	−582.844	−385.0347	−208.2995	−0.022750

References

[1] A. Rincón-Casado, J. González-Carbajal, D. García-Vallejo, J. Domínguez, Analytical and numerical study of the influence of different support types in the nonlinear vibrations of beams, Eur. J. Mech. A Solids 85 (2021) 104113, http://dx.doi.org/10.1016/j.euromechsol.2020.104113.

[2] S. Atluri, Nonlinear vibrations of a hinged beam including nonlinear inertia effects, J. Appl. Mech. 40 (1) (1973) 121–126, http://dx.doi.org/10.1115/1.3422909.

[3] D.A. Evensen, Nonlinear vibrations of beams with various boundary conditions, AIAA J. 6 (2) (1968) 370–372, http://dx.doi.org/10.2514/3.4506.

[4] S. Woinowsky-Krieger, The effect of an axial force on the vibration of hinged bars, J. Appl. Mech. 17 (1950).

[5] A.V. Srinivasan, Non-linear vibrations of beams and plates, Int. J. Non-Linear Mech. 1 (3) (1966) 179–191, http://dx.doi.org/10.1016/0020-7462(66)90003-5.

[6] S. Lenci, F. Clementi, G. Rega, A comprehensive analysis of hardening/softening behaviour of shearable planar beams with whatever axial boundary constraint, Meccanica 51 (11) (2016) 2589–2606, http://dx.doi.org/10.1007/s11012-016-0374-6.

[7] S. Lenci, G. Rega, Axial-transversal coupling in the free nonlinear vibrations of timoshenko beams with arbitrary slenderness and axial boundary conditions, Proc. Math. Phys. Eng. Sci. 472 (2190) (2016) 20160057, http://dx.doi.org/10.1098/rspa.2016.0057.

[8] L. Kloda, S. Lenci, J. Warminski, Nonlinear dynamics of a planar beam–spring system: analytical and numerical approaches, Nonlinear Dynam. 94 (3) (2018) 1721–1738, http://dx.doi.org/10.1007/s11071-018-4452-2.

[9] L. Kloda, S. Lenci, J. Warminski, Nonlinear dynamics of a planar hinged-simply supported beam with one end spring: Higher order resonances, in: I. Kovacic, S. Lenci (Eds.), IUTAM Symposium on Exploiting Nonlinear Dynamics for Engineering Systems, in: IUTAM Bookseries, vol. 37, Springer International Publishing, Cham, 2020, pp. 155–165, http://dx.doi.org/10.1007/978-3-030-23692-2_14.

[10] N. Araumi, H. Yabuno, Cubic–quintic nonlinear parametric resonance of a simply supported beam, Nonlinear Dynam. 90 (1) (2017) 549–560, http://dx.doi.org/10.1007/s11071-017-3680-1.

[11] A. Shibata, S. Ohishi, H. Yabuno, Passive method for controlling the nonlinear characteristics in a parametrically excited hinged-hinged beam by the addition of a linear spring, J. Sound Vib. 350 (2015) 111–122, http://dx.doi.org/10.1016/j.jsv.2015.03.055.

[12] L. Kloda, S. Lenci, J. Warminski, Hardening vs. softening dichotomy of a hinged-simply supported beam with one end axial linear spring: Experimental and numerical studies, Int. J. Mech. Sci. 178 (2020) 105588, http://dx.doi.org/10.1016/j.ijmecsci.2020.105588.

[13] W. Lacarbonara, H. Yabuno, Refined models of elastic beams undergoing large in-plane motions: Theory and experiment, Int. J. Solids Struct. 43 (17) (2006) 5066–5084, http://dx.doi.org/10.1016/j.ijsolstr.2005.07.018.

[14] A.H. Nayfeh, B. Balachandran, Modal interactions in dynamical and structural systems, Appl. Mech. Rev. 42 (11S) (1989) S175–S201, http://dx.doi.org/10.1115/1.3152389.

[15] A.H. Nayfeh, D.T. Mook, Nonlinear Oscillations, first ed., in: Physics Textbook, Wiley-VCH, Weinheim, 2008.

[16] F. Clementi, S. Lenci, G. Rega, 1:1 internal resonance in a two d.o.f. complete system: a comprehensive analysis and its possible exploitation for design, Meccanica 55 (6) (2020) 1309–1332, http://dx.doi.org/10.1007/s11012-020-01171-9.

[17] C.-M. Chin, A.H. Nayfeh, Three-to-one internal resonances in hinged-clamped beams, Nonlinear Dynam. 12 (2) (1997) 129–154, http://dx.doi.org/10.1023/A:1008229503164.

[18] C.-M. Chin, A.H. Nayfeh, Three-to-one internal resonances in parametrically excited hinged-clamped beams, Nonlinear Dynam. 20 (2) (1999) 131–158, http://dx.doi.org/10.1023/A:1008310419911.

[19] S.A. Emam, A.H. Nayfeh, Non-linear response of buckled beams to 1:1 and 3:1 internal resonances, Int. J. Non-Linear Mech. 52 (2013) 12–25, http://dx.doi.org/10.1016/j.ijnonlinmec.2013.01.018.

[20] A.H. Nayfeh, W. Kreider, T.J. Anderson, Investigation of natural frequencies and mode shapes of buckled beams, AIAA J. 33 (6) (1995) 1121–1126, http://dx.doi.org/10.2514/3.12669.

[21] A.H. Nayfeh, W. Lacarbonara, C.-M. Chin, Nonlinear normal modes of buckled beams: Three-to-one and one-to-one internal resonances, Nonlinear Dynam. 18 (3) (1999) 253–273, http://dx.doi.org/10.1023/A:1008389024738.

[22] H.M. Ouakad, H.M. Sedighi, M.I. Younis, One-to-one and three-to-one internal resonances in MEMS shallow arches, J. Comput. Nonlinear Dyn. 12 (5) (2017) 156, http://dx.doi.org/10.1115/1.4036815.

[23] G.A. Varzandian, S. Ziaee, M. Farid, A. Niknejad, Nonlinear vibration and stability analysis of thermally postbuckled double-layered graphene sheet under 1:1 and 3:1 internal resonance, Int. J. Struct. Stab. Dyn. 20 (04) (2020) 2050044, http://dx.doi.org/10.1142/S0219455420500443.

[24] G.-X. Wang, H. Ding, L.-Q. Chen, Gravitational effects and mode interactions of vertical cantilever beams, Int. J. Non-Linear Mech. 123 (2020) 103493, http://dx.doi.org/10.1016/j.ijnonlinmec.2020.103493.

[25] H. Arvin, A. Arena, W. Lacarbonara, Nonlinear vibration analysis of rotating beams undergoing parametric instability: Lagging-axial motion, Mech. Syst. Signal Process. 144 (6) (2020) 106892, http://dx.doi.org/10.1016/j.ymssp.2020.106892.

[26] H. Arvin, W. Lacarbonara, F. Bakhtiari-Nejad, A geometrically exact approach to the overall dynamics of elastic rotating blades—part 2: flapping nonlinear normal modes, Nonlinear Dynam. 70 (3) (2012) 2279–2301, http://dx.doi.org/10.1007/s11071-012-0619-4.

[27] B. Zhang, H. Ding, L.-Q. Chen, Three to one internal resonances of a pre-deformed rotating beam with quadratic and cubic nonlinearities, Int. J. Non-Linear Mech. 126 (2020) 103552, http://dx.doi.org/10.1016/j.ijnonlinmec.2020.103552.

[28] F.K. Alfosail, M.I. Younis, Multifrequency excitation of an inclined marine riser under internal resonances, Nonlinear Dynam. 99 (1) (2020) 149–171, http://dx.doi.org/10.1007/s11071-019-05136-w.

[29] J.L. Huang, R. Su, W.H. Li, S.H. Chen, Stability and bifurcation of an axially moving beam tuned to three-to-one internal resonances, J. Sound Vib. 330 (3) (2011) 471–485, http://dx.doi.org/10.1016/j.jsv.2010.04.037.
[30] S. Lenci, F. Clementi, L. Kloda, J. Warminski, G. Rega, Longitudinal–transversal internal resonances in Timoshenko beams with an axial elastic boundary condition, Nonlinear Dynam. 40 (11) (2020) 121, http://dx.doi.org/10.1007/s11071-020-05912-z.
[31] L. Kloda, Coupled Longitudinal–Transversal Vibrations of a Nonlinear Planar Timoshenko Beam with an Axial End Spring: Analytical Modeling, Numerical Simulation and Experimental Study (Ph.D. thesis), Polytechnic University of Marche, 2020.
[32] I.-S. Son, Y. Uchiyama, W. Lacarbonara, H. Yabuno, Simply supported elastic beams under parametric excitation, Nonlinear Dynam. 53 (1–2) (2008) 129–138, http://dx.doi.org/10.1007/s11071-007-9301-7.
[33] L. Kloda, S. Lenci, J. Warminski, Nonlinear dynamics of a planar hinged-supported beam with one end lumped mass and longitudinal elastic support, MATEC Web Conf. 241 (2018) 01016, http://dx.doi.org/10.1051/matecconf/201824101016.
[34] E. Babilio, S. Lenci, Consequences of different definitions of bending curvature on nonlinear dynamics of beams, Procedia Eng. 199 (2017) 1411–1416, http://dx.doi.org/10.1016/j.proeng.2017.09.382.
[35] A.H. Nayfeh, Introduction to Perturbation Techniques, Wiley-VCH Verlag GmbH & Co. KGaA, Weinheim (Germany), 2004.
[36] A.H. Nayfeh, Perturbation Methods, John Wiley & Sons, New York, 2011.
[37] L. Kloda, S. Lenci, J. Warminski, Nonlinear dynamics of a planar hinged-supported beam with one end spring system, MATEC Web Conf. 148 (6) (2018) 06004, http://dx.doi.org/10.1051/matecconf/201814806004.
[38] N. Andonovski, S. Lenci, Six-dimensional basins of attraction computation on small clusters with semi-parallelized SCM method, Int. J. Dyn. Control 8 (2) (2020) 436–447, http://dx.doi.org/10.1007/s40435-019-00557-2.
[39] H.E. Nusse, J.A. Yorke, Dynamics, second ed., in: Diskette of Applied Mathematical Sciences, vol. 101, Springer, New York and Berlin, 1998.